Discovery of orally active indirubin-3′-oxime derivatives as potent type 1 FLT3 inhibitors for acute myeloid leukemia

Pyeonghwa Jeong, Yeongyu Moon, Je-Heon Lee, So-Deok Lee, Jiyeon Park, Jungeun Lee, Jiheon Kim, Hyo Jeong Lee, Na Yoon Kim, Jungil Choi, Jeong Doo Heo, Ji Eun Shin, Hyun Woo Park, Yoon-Gyoon Kim, Sun-Young Han, Yong-Chul Kim

PII: S0223-5234(20)30172-0

DOI: https://doi.org/10.1016/j.ejmech.2020.112205

Reference: EJMECH 112205

To appear in: *European Journal of Medicinal Chemistry*

Received Date: 9 September 2019

Revised Date: 3 March 2020

Accepted Date: 3 March 2020

Please cite this article as: P. Jeong, Y. Moon, J.-H. Lee, S.-D. Lee, J. Park, J. Lee, J. Kim, H.J. Lee, N.Y. Kim, J. Choi, J.D. Heo, J.E. Shin, H.W. Park, Y.-G. Kim, S.-Y. Han, Y.-C. Kim, Discovery of orally active indirubin-3′-oxime derivatives as potent type 1 FLT3 inhibitors for acute myeloid leukemia, *European Journal of Medicinal Chemistry* (2020), doi: https://doi.org/10.1016/j.ejmech.2020.112205.

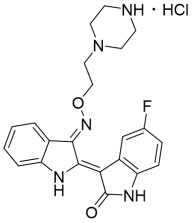

36

FLT3 IC_{50} = 0.87 nM
FLT3(D835Y) IC_{50} = 0.32 nM
MV4-11 GI_{50} = 1.0 nM
MOLM14 wt GI_{50} = 4.88 nM
MOLM14-FLT3-ITD GI_{50} = 1.85 nM
MOLM14-FLT3-ITD-D835Y GI_{50} = 1.87 nM
MOLM14-FLT3-ITD-D835Y GI_{50} = 3.27 nM
Oral Bioavailability = 42.6%
TGI (MV4-11, 20mg/kg/d p.o): Complete Remission

Type I Binding Mode

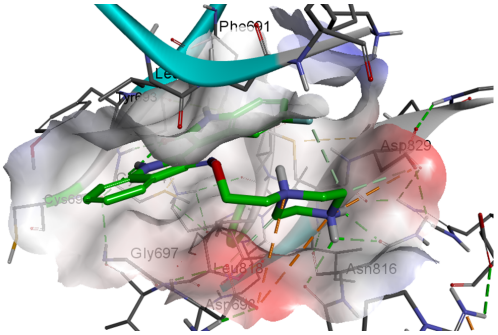

Discovery of Orally Active Indirubin-3′-oxime Derivatives as Potent Type 1 FLT3 Inhibitors for Acute Myeloid Leukemia

Pyeonghwa Jeong,[†] Yeongyu Moon, [§] Je-Heon Lee, [‡] So-Deok Lee, [‡] Jiyeon Park, [‡] Jungeun Lee, [‡] Jiheon Kim, [‡] Hyo Jeong Lee, [‖] Na Yoon Kim, [⊥] Jungil Choi, [§] Jeong Doo Heo, [§] Ji Eun Shin, [Δ] Hyun Woo Park, [Δ] Yoon-Gyoon Kim, [⊥] Sun-Young Han[*, ‖], Yong-Chul Kim[*,†,‡]

[†] Biomedical Science and Engineering, Gwangju Institute of Science and Technology, Gwangju, Republic of Korea

[‡] School of Life Sciences, Gwangju Institute of Science and Technology, Gwangju, Republic of Korea

[⊥]College of Pharmacy, Dankook University, Cheonan 330-714, Republic of Korea

[§] Gyeongnam Department of Environmental Toxicology and Chemistry, Korea Institute of Toxicology, Jinju, Gyeongsangnam-do 52834, Republic of Korea

[‖]College of Pharmacy and Research Institute of Pharmaceutical Sciences, Gyeongsang National University, Jinju, Gyeongsangnam-do 52828

[Δ]Department of Biochemistry, College of Life Science and Biotechnology, Yonsei University, Seoul 03722, Korea

Abstract

FMS-like receptor tyrosine kinase-3 (FLT3) is expressed on acute leukemia cells and is implicated in the survival, proliferation and differentiation of hematopoietic cells in most acute myeloid leukemia (AML) patients. Despite recent achievements in the development of FLT3-targeted small-molecule drugs, there are still unmet medical needs related to kinase selectivity and the progression of some mutant forms of FLT3. Herein, we describe the discovery of novel orally available type 1 FLT3 inhibitors from structure-activity relationship (SAR) studies for the optimization of indirubin derivatives with biological and pharmacokinetic profiles as potential therapeutic agents for AML. The SAR exploration provided important structural insights into the key substituents for potent inhibitory activities of FLT3 and in MV4-11 cells. The profile of the most optimized inhibitor (**36**) showed IC_{50} values of 0.87 and 0.32 nM against FLT3 and FLT3/D835Y, respectively, along with potent inhibition against MV4-11 and FLT3/D835Y expressed MOLM14 cells with a GI_{50} value of 1.0 and 1.87 nM, respectively. With the high oral bioavailability of 42.6%, compound **36** displayed significant in vivo antitumor activity by oral administration of 20 mg/kg once daily dosing schedule for 21 days in a mouse xenograft model. The molecular docking study of **36** in the homology model of the DFG-in conformation of FLT3 resulted in a reasonable binding mode in type 1 kinases similar to the reported type 1 FLT3 inhibitors Crenolanib and Gilteritinib.

Introduction

FMS-like receptor tyrosine kinase-3 (FLT3), a receptor tyrosine kinase (RTK) in the type III RTK family, is expressed on most acute leukemia cells and normal hematopoietic stem cells. The activation of FLT3 is initiated by the binding of the FLT3 ligand (FL), which is expressed in stromal cells. Upon stimulation with FL, FLT3 activation induces dimerization and conformational changes in the receptor as well as autophosphorylation of specific tyrosine residues, consequently triggering cascade signaling, including Ras/Raf, PI3K, AKT, STAT5, Grb2, SHP-2, SHIP, MAPK and ERK1/2. The downstream cascades from FLT3 can be categorized into the PI3K/AKT, RAS/MAPK, and STAT5 signaling pathways. [1, 2] Acute myeloid leukemia is a cancer of the myeloid line of blood cells, characterized by the rapid growth of abnormal blood cells originating from bone marrow, interfering with normal blood cells. [3] AML is the most common form of acute leukemia that generally occurs in the elderly patient population and is responsible for half of pediatric leukemia mortality. [4, 5] Recently, genomic sequencing analysis has identified that mutations commonly appearing in the signaling genes led to FLT3, which has been consequently studied as an attractive therapeutic target for AML. [6, 7] Two broad types of FLT3 mutations have been identified: internal tandem duplication (ITD) mutations [8] and point mutations in the tyrosine kinase domain (TKD), typically at the activation loop (AL) residue D835. [9]

In recent decades, a number of small molecule inhibitors have been reported for AML, such as Sunitinib, [10] Midostaurin, [11] Sorafenib, [12] Tandutinib, [13] Quizartinib, [14] Ponatinib, [15] Crenolanib, [16] and Gilteritinib [17] (Figure 1). However, most of these inhibitors showed multikinase inhibitory activities that limit their potency and repositioning for the treatment of AML with the FLT3 mutation.[11, 18, 19] Moreover, the occurrence of drug resistance due to the FLT3/TKD mutation during chemotherapy represents a challenge

to successful FLT3 inhibition. [20] Therefore, the development of potent and selective FLT3 kinase inhibitors, especially those effective for resistant AML caused by mutations, is in high demand to solve the unmet medical needs of AML monotherapy.

Indirubin core skeleton has been extensively studied for the development of effective kinase inhibitors,[21] [22] such as CDK and GSK3b. Our group also previously reported several indirubin-3`-oxime derivatives as potent FLT3[23] and CDK inhibitors[24] depending on the substitutions at the 5 and 5` positions, which have indicated the versatile utilities of the skeleton toward particular class of kinase inhibitors. Recently, we also reported an indirubin derivative, compound **9** (Figure 1), which has potent inhibitory activity against FLT3 (IC_{50} = 3 nM) and the proliferation of MV4-11 cells (GI_{50} = 1 nM) with limited pharmacokinetic profiles. [25] Aiming the druggable physicochemical properties maintaining FLT3 inhibitory activities, herein, we report more optimized 5,5`-substituted indirubin analogs with additional pharmacophores at the 3`-oxime moiety starting from previously reported derivatives. [24] The biological profiles of compounds along with the oral bioavailability were evaluated, including FLT3 inhibition, anti-proliferative activity in the AML cell line and in vivo anticancer efficacy in a xenograft animal model by oral administration.

Figure 1. Chemical structures of FLT3 kinase inhibitors

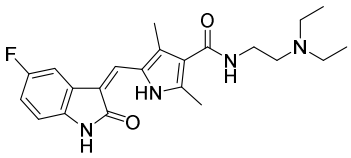

1 Sunitinib (FLT3 IC_{50} = 25 nM)

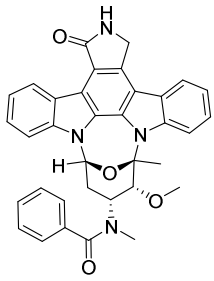

2 Midostaurin (FLT3 IC_{50} = < 10 nM)

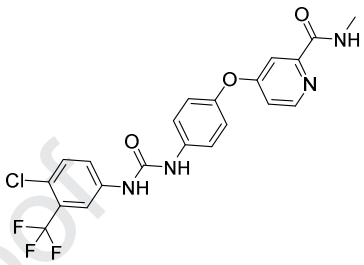

3 Sorafenib (FLT3 IC_{50} = 58 nM)

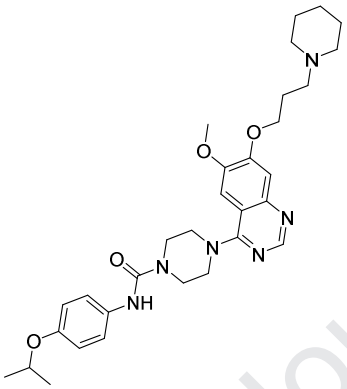

4 Tandutinib (FLT3 IC_{50} = 220 nM)

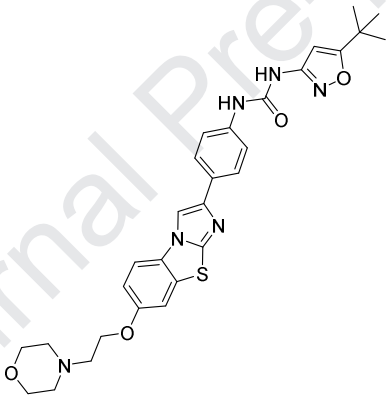

5 Quizartinib (FLT3 IC_{50} = 1.1 nM)

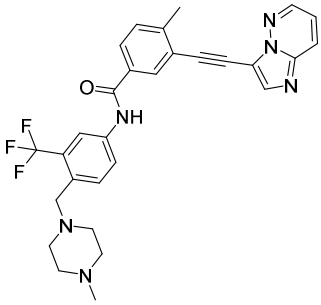

6 Ponatinib (FLT3 IC_{50} = 13 nM)

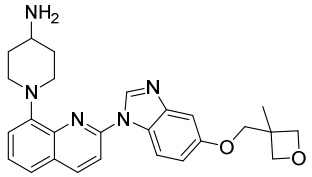

7 Crenolanib (FLT3 IC_{50} = 1.3 nM)

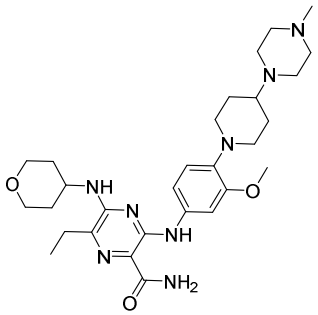

8 Gilteritinib (FLT3 IC_{50} = 0.29 nM)

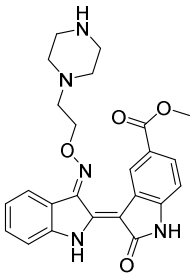

9 LDD1937 (FLT3 IC_{50} = 3 nM)

RESULT AND DISCUSSION

Chemistry

The synthesis of indirubin 3`-oximes **16a**, **17a-e**, and **18a-b** was performed following the synthetic routes represented in **Scheme 1**.

Scheme 1. General Synthetic Pathway of the Preparation of Indirubin 3′-oximes

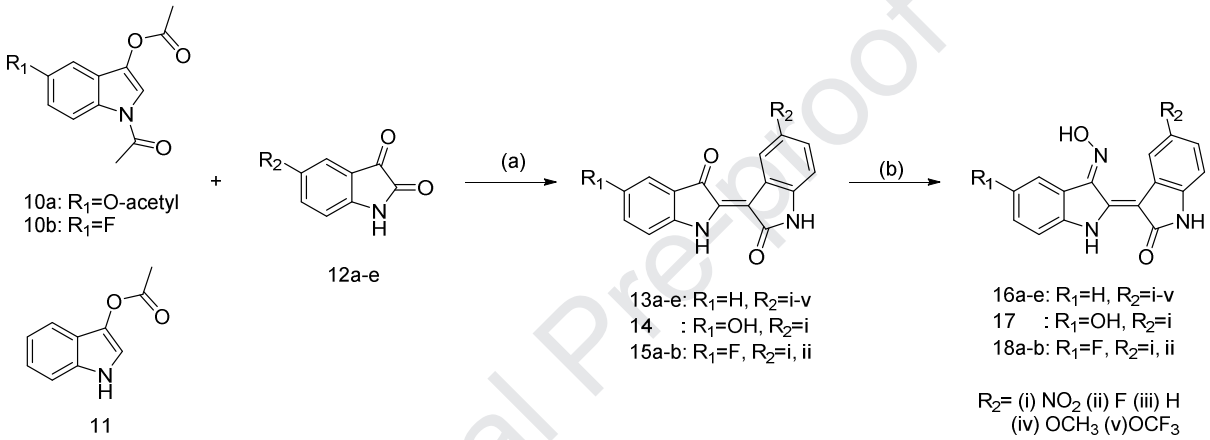

Reagents and conditions: (a) Na_2CO_3, methanol or methanol:water(2:1), RT, 2-3 h, 42-55%; (b) Hydroxylamine hydrochloride, pyridine, reflux, 3 h, 60-70%;

As our group reported in the previous study, we have included the process of making the final product in HCl salt form to solve the solubility problem of the indirubin derivative. To synthesize the 5,5'-substituted indirubin 3-oxime derivatives, the 5-substituted indoxyl-N,O-diacetates **10a-b** were prepared from their corresponding 5-substituted anthranilic acids.[24] For the 5-hydroxy analog, the cyclized compound **10a** was obtained as a triacetate form because the phenolic hydroxyl group was also acetylated under cyclization conditions. The 5,5'-substituted-3-indirubin oxime derivatives **16a, 17a-e**, and **18a-b** were synthesized from conjugate reactions of the 5-substituted indoxyl-N,O-diacetates **10a-b** or **11** with various isatins (**12a-e**) under basic conditions to yield the 5,5′-substituted indirubin

derivatives **13a, 14a-e, and 15a-b,** followed by the reaction of each of the latter with hydroxylamine to convert the ketone group to an N-oxime.

Scheme 2. Synthetic of Compounds 20 and 24-29

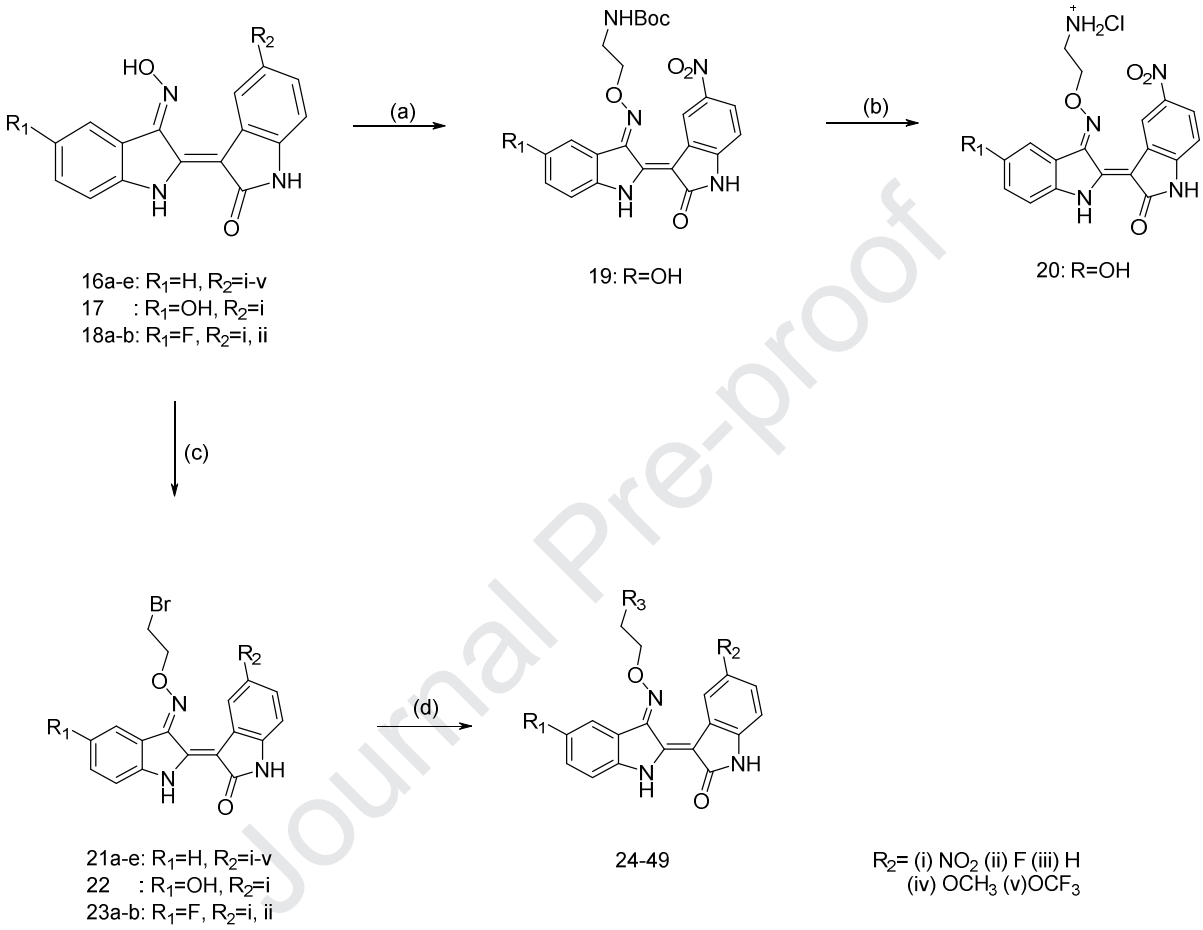

Reagents and conditions: (a) 2-(boc-amino)ethyl bromide, K_2CO_3, DMF, RT, overnight; (b) 4N HCl in 1,4-dioxane, DCM, 0 □, 3 h; (c) 1,2-dibromoethane, Et_3N, DMF, RT, overnight; (d) Various amines, DMF, 50 □, overnight; *then* 4N HCl in 1,4-dioxane, THF, 0 □, 30 min;

Scheme 2 presents the synthetic routes for compounds **20** and **24-50**. Reaction of 5-hydroxy-5-nitro indirubin 3-oxime (**16a**) with 2-(Boc-amino)ethyl bromide gave intermediate

compound **19**, which was subjected to a sequence of reactions, including deprotection of the Boc protecting group followed by HCl salt formation to yield compound **20**. Compounds **21a-e, 22**, and **23a-b** were obtained using the O-alkylation process between 1,2-dibromoethane and N-oxime compounds **16a, 17a-e, and 18a-b,** respectively. The terminal bromides of **21a-e, 22** and **23a-b** were coupled with various heterocyclic compounds containing amino moieties under basic conditions to afford the corresponding intermediates, which were then treated with 4 N HCl in dioxane to yield the desired final compounds **24-49** in excellent yield.

Structure-Activity Relationships with Pharmacokinetic Studies

The biological activities of the synthesized indirubin derivatives were evaluated for their inhibitory activities against FLT3 and the proliferation of MV4-11 cells, an FLT3-ITD positive AML cell line using the WST assay protocol. In our previous report, [24] potent CDK inhibitors with the indirubin skeleton were discovered, including compound **17** (IC_{50} = 1.9 nM for CDK2), which was further identified as an inhibitor of FLT3 (IC_{50} = 23.4 nM), showing moderate antiproliferative activity against MV4-11 cells (GI_{50} = 133 nM, Table 1). [23] We have also reported that the introduction of heterocyclic moieties on the 3`-oxime position (R3) led to a significant increase in the potency against both FLT3 and MV4-11 cells. [25] Also, the docking analysis with a nitro group at the R2 position such as the case of compound **24** resulted in the sufficient numbers of interactions in the ATP binding site of FLT3. (See supporting information) Therefore, to improve the inhibitory potency of compound **17** against FLT3, we introduced several functional groups with ethyl linkers at the R3 position of compound **17** (**20**-**26**, Table 1).

Table 1. Biological Activities of compound **17, 20, 22** and **24-35** against FLT3 and MV4-11 Cells

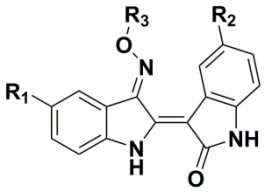

Compound	R_1	R_2	R_3	IC_{50} (nM)	GI_{50} (nM)
				FLT3[a]	MV4;11[b]
17	OH	NO_2	H	23.4 ± 1.06	133 ± 19.9
20	OH	NO_2	$CH_2CH_2NH_2 \cdot HCl$	8.6 ± 1.22	95.3 ± 10.3
22	OH	NO_2	CH_2CH_2Br	324 ± 42.4	470 ± 86.1
24	OH	NO_2	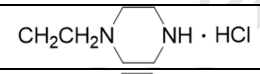	12.2 ± 1.64	26.5 ± 11.1
25	OH	NO_2	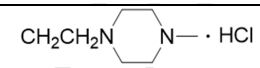	18.9 ± 3.53	50 ± 16.6
26	OH	NO_2	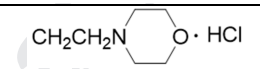	345 ± 93.8	100 ± 10.9
27	F	NO_2	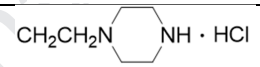	27.6 ± 2.77	10.2 ± 2.33
28	F	NO_2	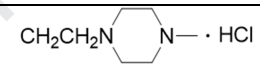	31.2 ± 5.06	118 ± 28.1
29	H	NO_2	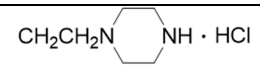	13.2 ± 0.87	7.01 ± 1.90
30	F	F	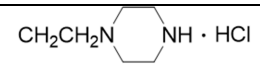	15.8 ± 1.46	8.3 ± 1.73
31	F	F	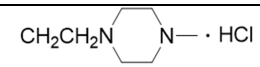	27.0 ± 2.58	31.5 ± 8.8
32	F	F	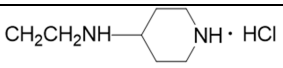	11.6 ± 1.05	8.4 ± 2.93
33	F	F	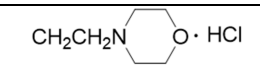	98.3 ± 17.6	115.5 ± 16.5
34	F	F	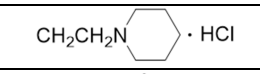	45.0 ± 1.19	105.3 ± 43.3
35	F	F	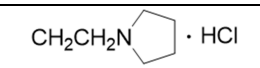	116 ± 1.11	633.9 ± 173
Lestaurtinib				3	33

[a]IC_{50} = 50% inhibitory concentrations of FLT3 were obtained from dose-dependent response curves.

[b]GI_{50} = 50% inhibitory concentrations of cell proliferation were obtained from dose-dependent response curves. All biological data were obtained in triplicate and presented as the mean mean ± standard error of the mean (SEM)

Substitutions to the R3 moiety with an amino ethyl moiety (**20**) resulted in more potent inhibitory activity compared to compound **17** (IC_{50} = 8.60 nM vs 23.4 nM and GI_{50} = 95.3 nM vs 133 nM, respectively). In contrast, the corresponding bromo ethyl derivative (**21**) of compound **20** showed a drastic loss in FLT3 inhibitory activity as well as MV4-11 antiproliferative efficacy (IC_{50} = 324 nM and GI_{50} = 470 nM, respectively), suggesting that the basic properties at this position play an important role in optimizing the biological activity. Thus, compounds **24** and **25** with piperazine and N-methyl piperazine moieties substituted for the bromo moiety of compound **22**, respectively, exhibited 10- to 20-fold enhanced potencies for FLT3 and MV4-11 (IC_{50} = 12.2 nM, 18.9 nM and GI_{50} = 26.5 nM, 50 nM, respectively). When the piperazine ring was replaced with a morpholine ring (**26**) at the R3 position, both FLT3 inhibitory activity (IC_{50} = 345 nM) and MV4-11 antiproliferative activity (GI_{50} = 100 nM) significantly decreased, indicating that the terminal amine of the heterocyclic ring may be beneficial.

Among the series of compounds **20**-**26**, we evaluated the pharmacokinetic (PK) properties of compounds **20** and **24** in mice by intravenous or oral administration. The relevant pharmacokinetic parameters are described in Supporting Table 1. The results demonstrated poor oral bioavailability (F = 0% and 0% for **20** and **24**, respectively) and rapid clearance (CL_{obv} = 10,379 and 70.4 mL/min/kg, respectively) of compounds **20** and **24**, respectively. The poor PK profiles might be due to metabolically labile groups, such as hydroxyl and nitro groups.

Next, to improve the FLT3 inhibitory activities and pharmacokinetic (PK) profiles, the hydroxyl and nitro groups at the R1 and R2 positions was further modified to fluorine or hydrogen groups based on our previous report, in which hydrogen and fluorine groups at the R1 and R2 position showed beneficial effects for the FLT3 inhibition. [23] As the results,

compounds **27** and **28** displayed slightly decreased activity against FLT3 (IC_{50} = 27.6 nM and 31.2 nM, respectively). Compound **29,** with a hydrogen at the R1 position, maintained its inhibitory potency against FLT3 (IC_{50} = 13.2 nM). These results indicate that fluorine or hydrogen the substituents at the R1 position along with nitro group at R2 position, may minimally affect for the FLT3 inhibitory activity. Interestingly, compounds **27** and **29** displayed increased MV4-11 anti-proliferative efficacy.

In the evaluation of the PK profiles of compound **29** without the hydroxyl group at the R1 position, disappointingly, poor oral bioavailability (F = 1.33%) and rapid clearance (CL_{obv} = 108 mL/min/kg) was observed. (Supporting Table 1) Therefore, it is expected that the poor PK profiles might be due to the nitro group at R2 position.

To further improve the PK profile while maintaining the biological activity, we next prepared 5,5`-difluoro indirubin derivatives **30**-**35** (Table 1). Among them, compounds **30** and **32** containing piperazine and 4-amino piperidine, respectively, at the R3 position showed the best potency with a low nanomolar range of biological activities either in the FLT3 assay or in MV4-11 cells (IC_{50} = 15.8 and 11.6 nM and GI_{50} = 8.30 and 8.47 nM, respectively). Comparing this series of derivatives, the morpholine, piperidine, and pyrrolidine-containing compounds (**33**, **34** and **35**) displayed 2- to 7-fold less inhibitory activity against FLT3 than the heterocyclic ring derivatives containing terminal nitrogens, such as piperazine, N-methyl piperazine and 4-amino piperidine (**30**, **31**, and **32**, respectively).

Next, the PK profiles of **30** and **32** were determined in mice by intravenous or oral administration (Supporting Table 2). Significant improvement, compared with **20**, **24**, and **29**, was achieved for oral bioavailability (F = 16.7 and 15.3%, respectively), with the suitable PK parameters of half-life ($T_{1/2}$ = 3.4 and 9.2 h, respectively) and clearance (CL_{obv} = 28.1 and 231 mL/min/kg, respectively). Thus, fluoro substitutions for either the hydroxyl or nitro

groups at the R1 and R2 positions are tolerable for maintaining the biological activity, and more importantly, granting improved oral PK profiles.

Table 2. Biological Activities of compound **36-49** against FLT3 and MV4-11 Cells

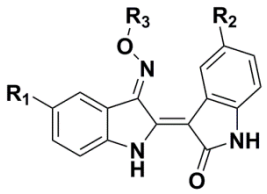

Compound	R_1	R_2	R_3	IC_{50} (nM)	GI_{50} (nM)
				FLT3[a]	MV4;11[b]
36	H	F	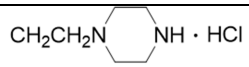	0.87 ± 0.16	1.0 ± 0.3
37	H	F	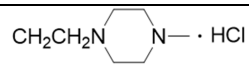	3.3 ± 1.27	11.1 ± 0.37
38	H	F	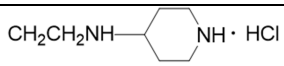	9.47 ± 0.31	11.9 ± 0.26
39	H	F	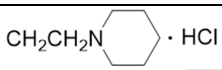	142 ± 7.07	263.3 ± 43.1
40	H	F	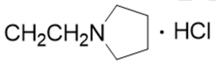	257 ± 44.2	212 ± 65.4
41	H	H	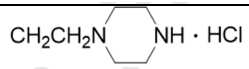	2.7 ± 1.10	0.51 ± 0.016
42	H	H	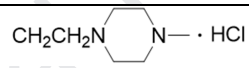	9.29 ± 2.77	54.8 ± 21.5
43	H	H	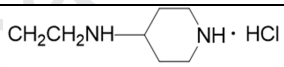	20.9 ± 2.88	15.1 ± 3.18
44	H	H	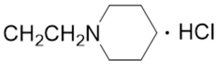	128 ± 22.5	138 ± 29.4
45	H	H	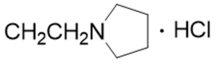	41.3 ± 2.68	103.5 ± 18.0
46	H	OCH_3	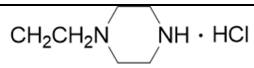	12.4 ± 1.08	22.0 ± 5.0
47	H	OCH_3	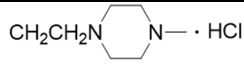	2.1 ± 1.14	20.0 ± 8.3
48	H	OCF_3	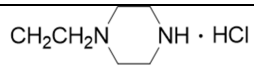	40.2 ± 1.13	17.0 ± 5.1
49	H	OCF_3	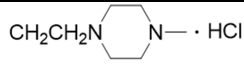	5.62 ± 1.05	7.0 ± 3.0
Lestaurtinib				3	33

[a]IC_{50} = 50% inhibitory concentrations of FLT3 were obtained from dose-dependent response curves.

[b]GI_{50} = 50% inhibitory concentrations of cell proliferation were obtained from dose-dependent response curves. All biological data were obtained in triplicate and presented as the mean mean ± standard error of the mean (SEM)

Since the above results from compounds **30** and **32** provided clues to achieve oral bioavailability, further optimization of the biological efficacy toward single-digit nanomolar IC_{50} values was attempted by modification of the substituents at the R1 and R2 positions (Table 2). Thus, the piperazine and N-methyl piperazine derivatives with no substitution at the R1 position (**36** and **37**) showed a dramatic increase in the potency compared with the corresponding fluoro analogs **30** and **31**, with IC_{50} values of 0.87 and 3.3 nM for the inhibitory activities of **36** and **37** against FLT3, respectively, along with an impressive enhancement of MV4-11 anti-proliferation activity, with GI_{50} values of 1.0 and 11.1 nM, respectively. In the case of compound **38** containing the ethyl(4-amino-piperidine) moiety at the R3 position, the activities against FLT3 and MV4-11 compared to corresponding compound **32** were similarly maintained (IC_{50} = 9.47 versus 11.6 nM and GI_{50} = 11.1 versus 8.47 nM for **38** and **32**, respectively). In contrast, the biological activities of compounds **39** and **40** with ethyl piperidine and ethyl pyrrolidine moieties at R3 position, respectively, were significantly decreased for their inhibitory activities against FLT3 (IC_{50} = 142 nM and 257 nM, respectively) and anti-proliferative efficacies against MV4-11 (GI_{50} = 263 nM and 212 nM, respectively).

We further removed the fluoro groups at the R2 position of **36-40** resulting in compounds **41-45**, to compare the electronic effects between fluorine and hydrogen at the R2 position. Among them, compounds **41-43**, containing piperazine, N-methyl piperazine and 4-amino piperidine moieties at the R3 position, respectively, displayed generally decreased inhibitory activities against FLT3 (IC_{50} = 2.7, 9.3 and 21 nM, respectively) and MV4-11 cells (GI_{50} = 0.51, 55 and 15 nM, respectively). Following similar activity profiles in the above cases, piperidine and pyrrolidine derivatives **44** and **45** exhibited a large decrease in inhibitory activity compared to **41**.

Next, we examined the effect of another functional groups at the R2 position by introducing methoxy or trifluoromethoxy moieties (**46**, **47**, **48**, and **49**), which possess a similar size but different electronic properties. In general, the methoxy derivatives **46** and **47** showed slightly more potent inhibitory activity against FLT3 compared to the corresponding trifluoromethoxy analogs **48** and **49**. Interestingly, unlike the SAR patterns of the previously discussed compounds, the N-methyl piperazine-containing compounds **47** and **49** were more potent than the corresponding piperazine derivatives **46** and **48**.

Next, two of the most active compounds, **36** and **41**, were subjected to PK profile investigations, with an intravenous or oral administration of a 10 mg/kg dose of the compounds in mice (**Figure 2** and **Supporting Table 3**). The results showed that **36** had an AUC_{last} of 25.0 μg·min/mL, a C_{max} of 36.5 ng/mL, and a remarkable increase in the oral bioavailability of 42.6%. The PK study of compound **41** also achieved satisfactory results, with an AUC_{last} of 72.1 μg·min/mL, a C_{max} of 69.7 ng/mL, and a bioavailability (F) of 51.0%.

As the consequences, we have successfully discovered orally administrable compounds with more potent FLT3 inhibitory activities and MV4-11 antiproliferative effects than the previously reported inhibitor with same skeleton, compound **9**. [25] Especially, the oral bioavailability (BA) of compounds **36** and **41** (BA = 42.6% and 51.0%, respectively) was greatly improved compared with compound **9** (BA = 1.43%)

Figure 2. The mean plasma concentration-time profiles of **36** and **41**. (A) Oral administration to ICR mouse of **36** at dose of 10 mg/kg (n=5) (B) Intravenous administration to ICR mouse of **36** at dose of 10 mg/kg (n=4) (C) Oral administration to ICR mouse of **41** at dose of 10 mg/kg (n=5) (D) Intravenous administration to ICR mouse of **41** at dose of 10 mg/kg (n=5). All data were obtained in triplicate and the error bars represent the standard error of the mean.

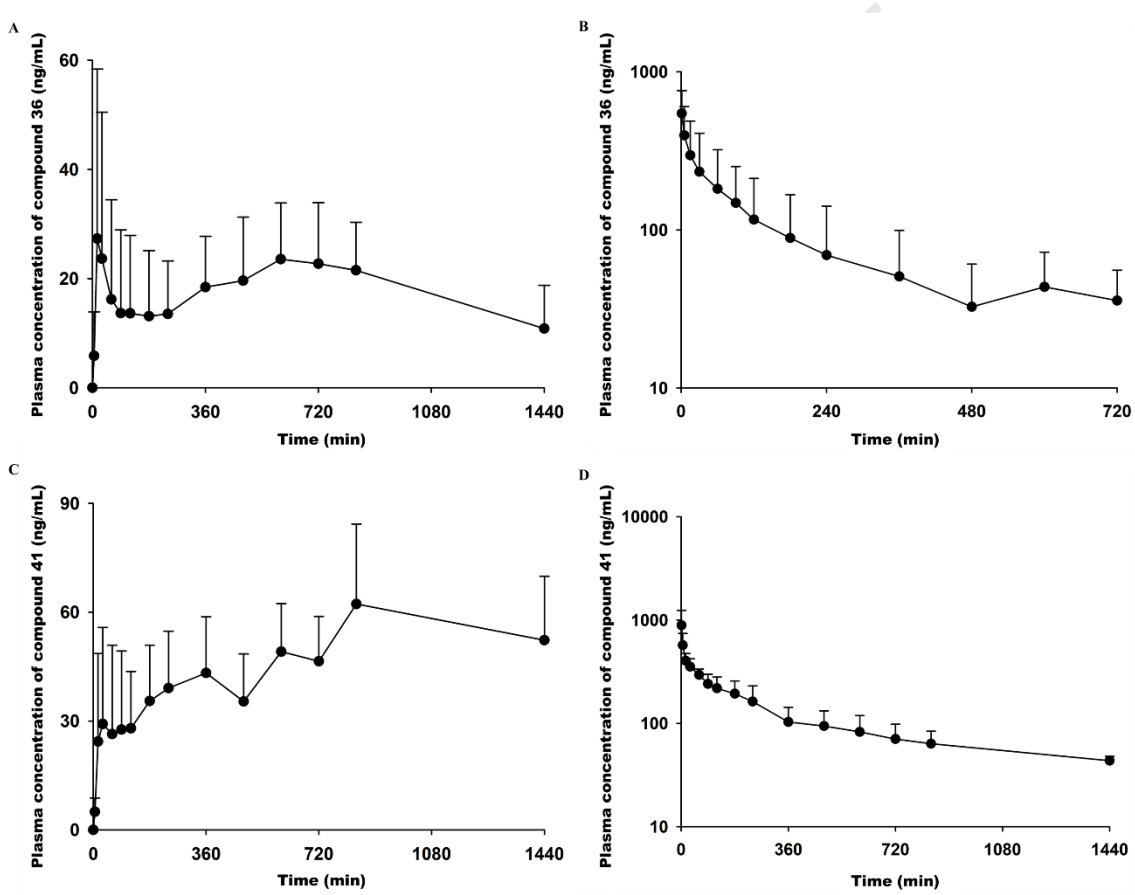

In conclusion, from the SAR analysis and PK optimization of the series of derivatives in Tables 1 and 2, the ethyl piperazine moiety at the R3 position and the fluoro moiety at the R2 position, such as the case of compound **36**, are the best combination for the highly potent FLT3 inhibitory activity along with MV4-11 anti-proliferative efficacy. In

addition, the PK profiles, including oral bioavailability, were critically dependent on the substituents at the 5 and 5`-positions (R1 and R2). For example, the oral bioavailability dramatically decreased depending on the substituent at the R1 and R2 positions in the following order: -H, -F < -F, -F < -H, -NO_2 < -OH, -NO_2, respectively.

Kinase Selectivity Assay

To investigate kinase selectivity profiles, we screened a single concentration of 100 nM of compound **36** against a Eurofins broad oncology panel of 104 kinases (**Figure 3**).

Figure 3. Kinase selectivity profiles of **36**. (A) Kinase tree illustration of compound **36** using KinMap. Kinase tree indicates the % inhibition value at 100 nM of compound **36** with concentration of ATP near to the K_m value for each individual target kinases. The red circle indicates kinases that were inhibited > 50%. Size of red circle is proportional to the % inhibition value. (B) Biological activities of **36** against other kinases.

A

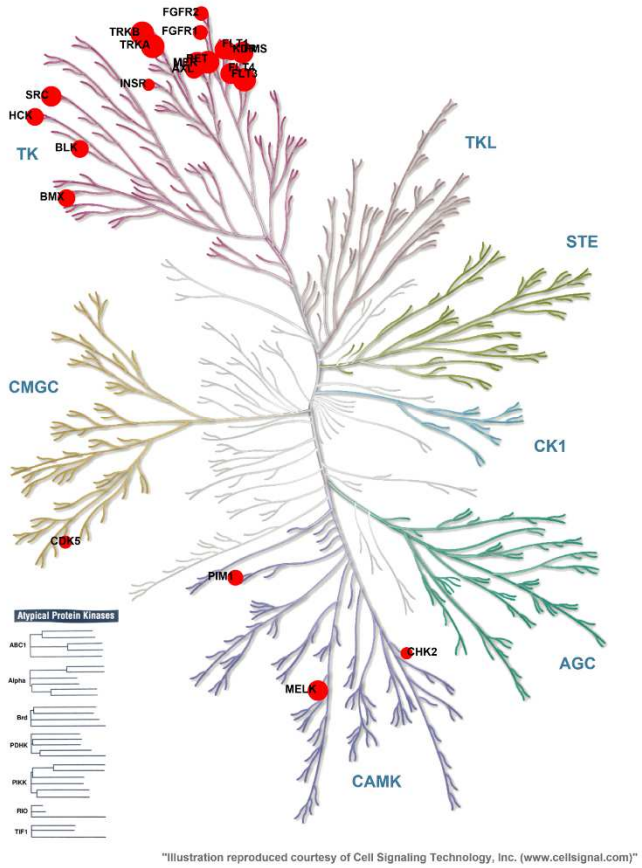

B

Kinase	% Inhibition	IC_{50} (nM)
FLT3	98	0.87
FLT3(D835Y)	99	0.32
FLT3-ITD	-	< 0.25 (K_d)
c-KIT	22	-
PDGFRα	5	-
Fms	92	4.20
Mer	100	3.01
Ret	98	1.21
TrkA	99	6.89
TrkB	100	2.04
cSRC	87	9.52
FLT4	89	23.8
MELK	86	5.54
CDK1	21	-
CDK2	43	-
CDK5	54	-

The kinome tree is illustrated in Figure 3A using KinMap, showing major selective inhibitory activities at the tyrosine kinase family with more than 90% inhibition such as FLT3/D835Y, FLT4, cSRC, Fms, Mer, Ret, TrkA, TrkB. [26] Remarkably, the inhibition of the mutant FLT3/D835Y (0.32 nM) turned out to be more potent than that of the wild type FLT3 (IC50 = 0.87 nM). Moreover, compound **36** displayed strong binding affinity at FLT3-ITD with a K_d value of < 0.25 nM. In contrast, kinases PDGFRα and c-KIT (Type 3 RTK),

which are typically inhibited by current FLT3 inhibitor drugs, [13, 27, 28] were weakly inhibited at 5% and 22%, respectively. In addition, compound **36** demonstrated selective inhibitory activities for FLT3 over the CDKs (21%, 42% and 54% inhibition against CDK1, CDK2 and CDK5 at 100 nM, respectively), even though indirubin derivatives have been reported as well-known CDK inhibitors. [22, 29-31] Recently, c-KIT inhibition of TKIs was reported as an important toxicological index associated with the disruption of hematopoietic progenitor cells related to myelosuppression.[28] In our case, an important, focused selectivity profile of weak c-KIT inhibition by compound **36** was observed, indicating that the possible hematopoietic toxicity associated with c-KIT could be avoided. The current FLT3-targeted drugs Quizartinib, Tandutinib, Crenolanib and Gilteritinib [32] have been reported with different kinase selectivity profiles. The analysis of the kinase selectivity profile of compound **36** in **Figure 3** demonstrated that the selective inhibitory activities are focused on the class of the tyrosine kinase family.

Cell Activity Evaluation of Compound 36

Since the FLT3 and FLT3(D835Y) inhibitory activities and the binding affinity for FLT3-ITD of compound **36** were determined as sub-nanomolar range of IC_{50} and K_d values (0.87 nM 0.32 nM and < 0.25 nM, respectively), the anti-proliferative activities of compound 36 were assessed against several FLT3-ITD positive human AML cell line including MOLM14 wild type, other clinically relevant mutant kinase expressed MOLM14 FLT3-ITD-site direct mutagenesis (MOLM14-ITD), MOLM14 FLT3-ITD- D835Y (MOLM14-ITD-D835Y) and MOLM14 FLT3-ITD-F691L (MOLM14-ITD-F691L) cells that are FLT3 growth dependent (**Figure 4**).

Figure 4. Anti-proliferative activities of compound 36 against MOLM14 mutant cells.

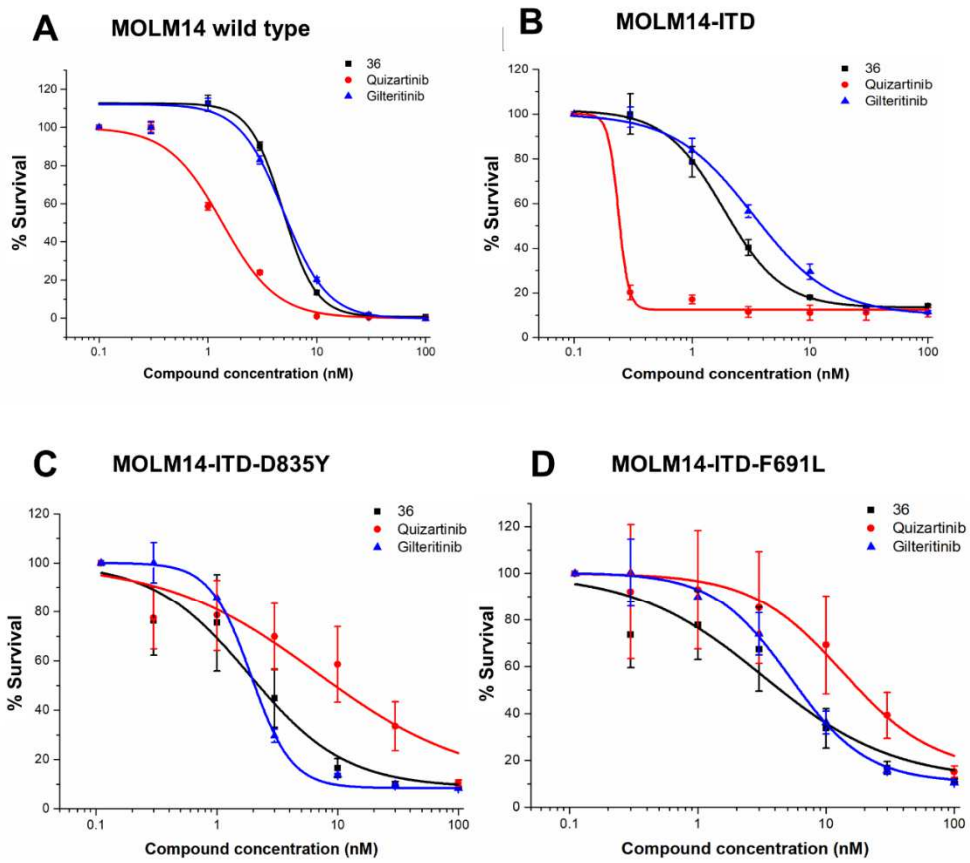

E

Compound	GI_{50} (nM)			
	MOLM14 wild type	MOLM14 - ITD	MOLM14 - ITD D835Y	MOLM14 - ITD F691L
36	4.88 ± 0.67	1.85 ± 0.06	1.87 ± 0.36	3.27 ± 0.99
Quizartinib	1.35 ± 0.11	0.23 ± 0.07	6.72 ± 2.28	13.58 ± 1.97
Gilteritinib	4.94 ± 0.65	3.29 ± 0.25	1.91 ± 0.07	5.24 ± 0.23

(A) Anti-proliferative activities of compound 36 against MOLM14 wild type cell line. (B) Anti-proliferative activities of compound 36 against MOLM14-ITD site direct mutagenesis cell line. (C) Anti-proliferative activities of compound 36 against MOLM14-ITD-D835Y cell line. (D) Anti-proliferative activities of compound 36 against MOLM14-ITD-F691L cell line.

(E) GI_{50} value of compound 36, Quizartinib and Gilteritinib against tested cell lines. All data ware obtained by triplet testing. For A-D, the error bar = SD.

In the same experiments, positive control drugs, Quizartinib and Gilteritinib which are representative type I and II inhibitor, respectively[33] were also tested in parallel. As the results, compound **36** showed similar dose-dependent anti-proliferative activity against MOLM14 wild type cell line with a GI_{50} values of 4.88 nM compared to Gilteritinib (GI_{50} = 4.94 nM) (**Figure 4A**). In addition, compound **36** was more sensitive to MOLM14-ITD cells (GI_{50} = 1.85 nM) than MOLM14 wild type with similar trend of Gilteritinib (**Figure 4B**). In the evaluation of the anti-proliferative effects against ITD-TKD dual mutant cell lines, MOLM14(FLT3-ITD, D835Y and F691L), compound **36** and the representative type I inhibitor, Gilteritinib, retained potent anti-proliferative effects against MOLM14 (FLT3-ITD, D835Y) dual mutant cells (GI_{50} = 1.87 nM and 1.91 nM, respectively) whereas type II inhibitor, Quizartinib, showed decreased inhibitory activity (GI_{50} = 6.72 nM) (**Figure 4C**). For MOLM14(FLT3-ITD, F691L) cell line, compound **36** and Gilteritinib also exhibited much higher anti-proliferative activities (GI_{50} = 3.27 nM and 5.24 nM, respectively) than that of Quizartinib (GI_{50} = 13.58 nM) (**Figure 4D**).

Selectivity Profiles of Compound 36 in Various Human Cancer Cell Lines

To evaluate the selective anti-proliferative activities of the representative compound **36** in the FLT3-ITD expressing AML cells, MV4-11, we examined WST assay to measure the cytotoxicity of compound **36** against several other cancer cell lines, including chronic myeloid leukemia (K562), lung cancer (A549), liver cancer (HepG2), triple negative breast cancer (MDA-MB-231), colon cancer (HCT-116), prostate cancer (PC3) and ovarian cancer

(SK-OV-3) compared with the positive control drug, Sorafenib and Gilteritinib. (**Table 3**) As the results, compound **36** showed 430 times more sensitive against MV4-11 cells (GI_{50} = 1 nM) than K562 cell line, which is insensitive to FLT3 inhibitors similar profile to Gilteritinib. Furthermore, compound 36 displayed good safety profiles against other cancer cell lines.

Table 3. Anti-proliferative Activities of Compound **36** Sorafenib and Gilteritinib against Various Cancer Cell Lines

Cell line	GI_{50} value (μM) or % inhibition at 1 μM[a]		
	36	Sorafenib	Gilteritinib
MV4-11	0.001 ± 0.0003	0.0009 ± 0.0001	0.0009 ± 0.0001[b]
K562	0.437 ± 0.038	0.612 ± 0.076	1.006 ± 0.263
A549	2.05 %	0 %	4.05 %
HepG2	1.1 ± 0.2	2.5 ± 0.5	2.2 ± 0.6
MDA-MB-231	8.95 %	5.45 %	42.13 %
HCT-116	38.46 %	11.01 %	45.10 %
PC3	40.67 %	32.98 %	41.76 %
SK-OV-3	16.04 %	4.51 %	23.33 %

[a] Compound **36**, Sorafenib and Gilteritinib were tested at 8 concentration to measure their anti-proliferative effects on various human cancer cell lines using WST assay. The GI_{50} values were obtained in triplicate and the error bars represent the standard error of the mean. [b] Reported GI_{50} value of Gilteritinib is 0.92 nM [34]

Compound 36 and 41 Inhibits the Phosphorylation of Proteins Downstream of FLT3

Compound **36, 41** and positive control Gilteritinib was further evaluated for its inhibitory activity of the downstream signal transduction pathway of FLT3 activation in MV4-11 cells at the concentrations of 1 μM, 100 nM and 10 nM (**Figure 5**).

Figure 5. Inhibition of STAT5 and Erk1/2 phosphorylation by compound **36**, **41** and Gilteritinib.

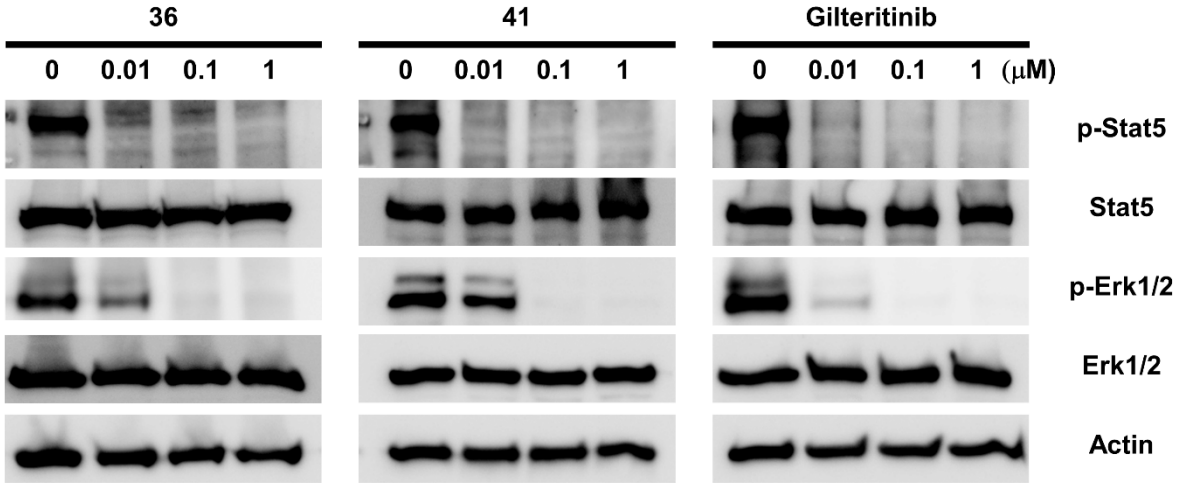

MV4-11 cells were treated with 10 nM, 100 nM and 1 μM of compound **36** for 4 hours. MV4-11 lysates were subjected to western blot analysis with indicated antibodies. Actin was used to probe for equal protein loading.

Compound **36** showed complete blockage of the phosphorylation of STAT5 even at the lowest test concentration, 10 nM, indicating the comparable functional activity resulted from

the FLT3 inhibition. Similarly, the phosphorylation of Erk1/2 was also strongly suppressed by compound **36**. Based on these results, the inhibition of downstream signal pathway of FLT3 autophosphorylation, occurring in FLT3-ITD expressing AML cell line, MV4-11, was confirmed compared with Gilteritinib, of which activity was obtained as similar to the reported data.[34]

Molecular Docking Study

To understand the binding mode of compound **36** in the kinase FLT3, we performed homology modeling and molecular docking studies at the ATP binding site of FLT3 using the Discovery Studio 3.5 program. Since the ligand-bound FLT3 cocrystal structures were reported only for inactive conformations with the DFG-out motif of the protein, current type 1 FLT3 inhibitors and compound **36** were not able to fit in the binding site. Therefore, to perform docking experiments for the type 1 inhibitors, homology protein models with DFG-in motifs were constructed using a previously reported method by Yi-Yu Ke et al. [35] Compound **36** along with the known FLT3 inhibitors Crenolanib and Gilteritinib were docked into the above FLT3 homology model using the CDOCKER protocol in the Discovery Studio 3.5 program.

Figure 6. Structural analysis of FLT3 inhibitors against the DFG-in FLT3 homology model. The compounds **36** and **39** were protonated in docking study. (A) 2D diagram of docking pose of **36**. Hydrogen bonds are indicated by red-hatched lines. Ionic interaction is indicated by brown-hatched line. Residues incorporating hydrophobic pocket in ATP binding site are noted in green color. Residues incorporating polar surface are noted in brown color. (B) Best docking pose of compound **36** into the homology model of DFG-in conformation of FLT3 (C) Docking pose of compound **38**. (D) Docking pose of compound **39**. (E) Docking pose of Crenolanib (E) Docking pose of Gilteritinib. In panel B to F, green and brown colors represent classical hydrogen bonding and ionic interaction respectively.

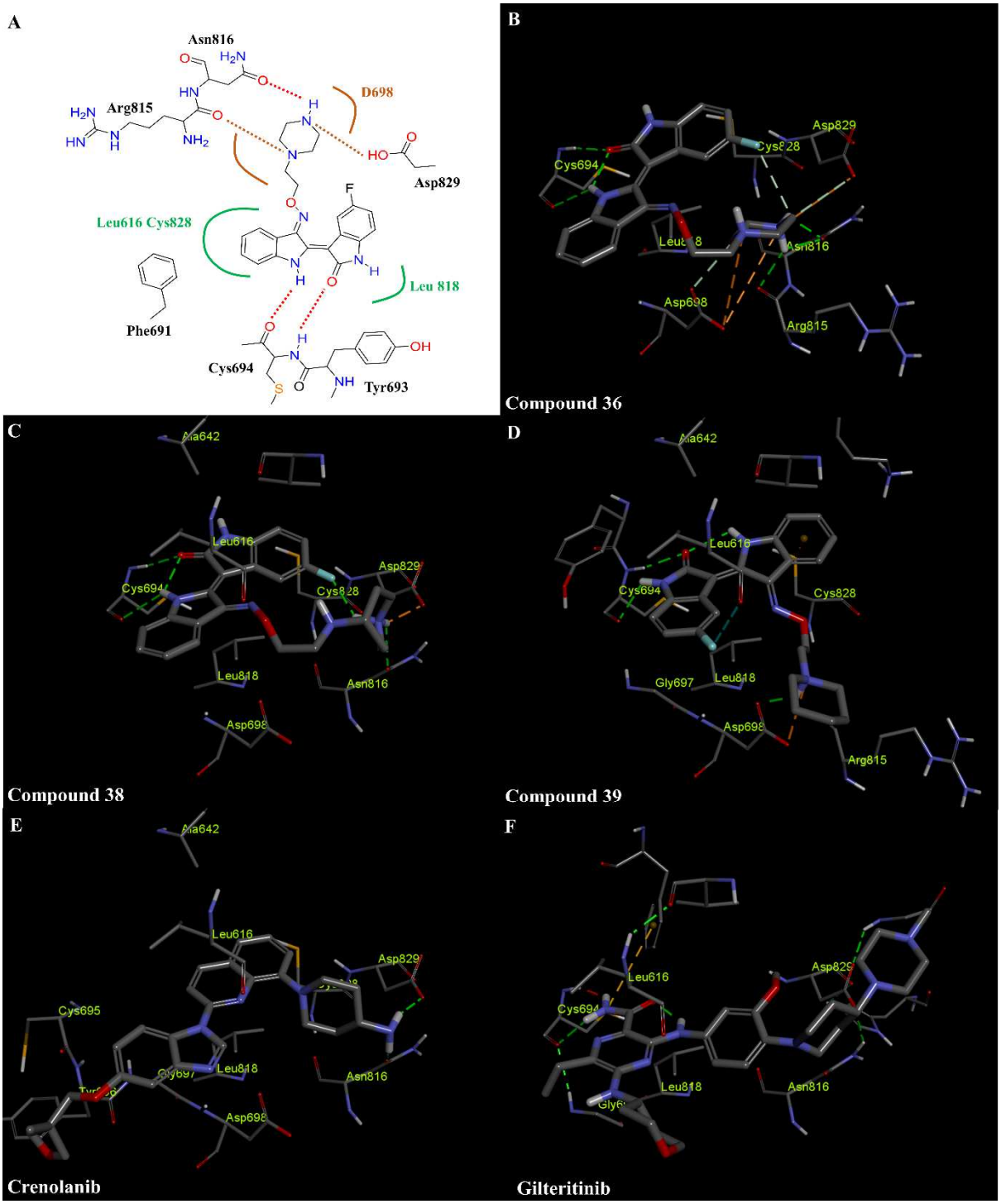
A
Asn816
Arg815
D698
Asp829
Leu616 Cys828
Leu 818
Phe691
Cys694
Tyr693
B
Asp829
Cys694
Asn816
Asp698
Arg815
Compound 36
C
Ala642
Leu616
Asp829
Cys694
Cys828
Leu818
Asn816
Asp698
Compound 38
D
Ala642
Leu616
Cys694
Cys828
Gly697
Leu818
Asp698
Arg815
Compound 39
E
Ala642
Leu616
Asp829
Cys695
Leu818
Asn816
Asp698
Crenolanib
F
Leu616
Asp829
Cys694
Leu818
Asn816
Gilteritinib

The docking results showed that compound **36** successfully docked into the ATP binding pocket, which was incorporated with hinge region and phosphate binding site of the FLT3. The detailed docking pose analysis of compound **36** using a 2D diagram is displayed in **Figure 6A**. There are two important hydrogen bonds formed between the backbone carbonyl and amino groups of the Cys694 residue with the secondary amine and carbonyl groups of the indirubin core scaffold of **36**. In addition, the aromatic portions of **36** were tightly surrounded by hydrophobic pockets consisting of the residues Leu616, Leu818, Cys828, and Tyr693. Interestingly, no interaction of compound **36** with gatekeeper residue F691 was observed, suggesting that **36** might be free from the concern of a mutation of F691. Another important pharmacophore, the piperazine moiety of **36**, may play important binding roles with the hydrophilic surface of phosphate binding pocket consisting of residues Asn816 and Asp829 of DFG motif. In particular, the tertiary amine of the piperazine moiety may form ion-dipole or ionic interactions with the backbone carbonyl group of Asn816 and the side chain of Asp698. In addition, the terminal amino group of piperazine may serve as a hydrogen bond donor to interact with the side chain of Asn816 and side chain of Asp829. (**Figure 6B**) In this binding model, the hydrogen bonding or ionic interactions of the nitrogen atoms in the piperazine of compound **36** with Asp698, Asn816 and Asp829 residue would play the critical roles for inhibitory activities from the analysis of the docking studies with less active compounds **38** and **39**. In the case of compound **38** (IC_{50} = 9.47 nM), the loss of interaction with Asp698 while maintaining the hydrogen bonding and ionic interaction with Asn816 and Asp829 residues, respectively, might result in the decreased inhibitory activity compared with compound **36** (IC_{50} = 0.87 nM). The docking analysis with much weaker derivative compound **39** (IC_{50} = 142 nM) suggested that the ethyl piperidine moiety of **39** headed to only Asp698 residue and solvent exposed area without the important interactions with Asn816 and Asp 829 residues. (**Figure 6D**) Therefore, the prediction of important

binding mechanism in the regions accommodating R3 moieties could be explained with the distinguished docking modes of the derivatives, **36**, **38** and **39** with different biological activities. The analysis and comparison of the docking poses of Crenolanib (**Figure 6E**) and Gilteritinib (**Figure 6F)** with those of **36** (**Figure 6B**) resulted in the conformational similarities of occupying the binding pocket. The piperazine moiety of compound **36**, the 4-amino piperidine moiety of Crenolanib, and the piperidinyl piperazine moiety of Gilteritinib showed common interactions with the polar surface of the FLT3 protein. Protein conformations, including the polar surface in several other kinases, are critical structural features for determining type 1 inhibitors and type 2 inhibitors. It has been reported that the ATP binding site containing the polar surface area is covered by the activation loop[35] in the inactive kinase conformation. [36-38] Overall, compound **36** turned out to fit well in our homology model of the active DFG-in conformation of FLT3, adopting the known structural features as a type 1 inhibitor similar to Crenolanib and Gilteritinib.

In vivo Anti-tumor Activity of Compounds 36 and 41

Figure 7. Anticancer efficacy in MV4-11 xenograft mouse model of compound **36** and **41**. (n = 10 for control group, n = 6 for test group) BALB/c nude mice bearing MV4-11 tumor xenograft were treated once daily with each compound at 20 mg/kg or vehicle. (A) Relative tumor size (B) Body weight measurement of MV4-11 xenograft mice after oral administration of compound **36** and **41**. (***, $p<0.001$)

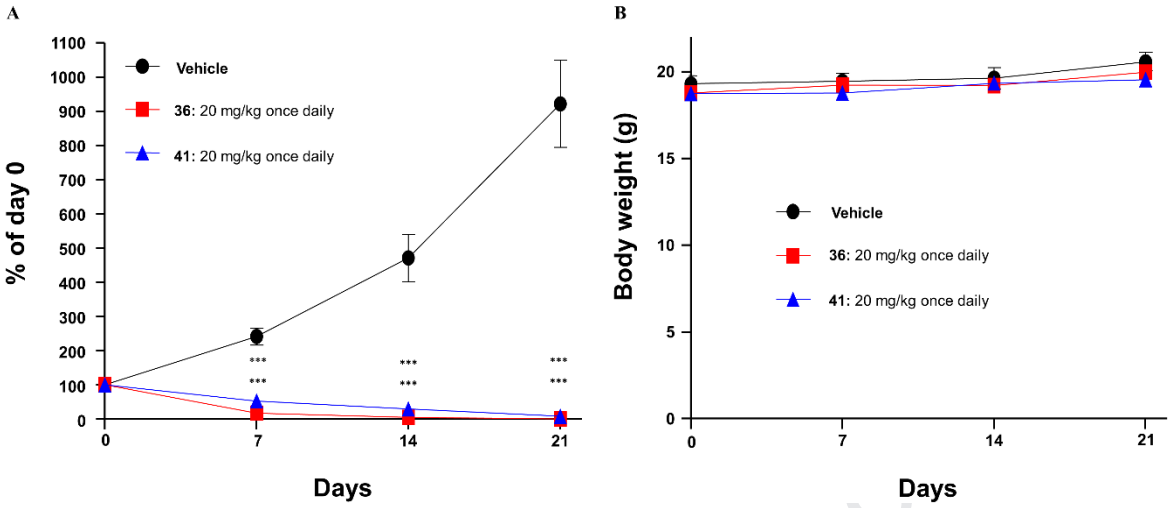

An in vivo MV4-11 xenograft study was performed to determine the efficacy of the indirubin derivatives. MV4-11 cells were subcutaneously injected into BALB/c nu/nu mice, and tumors were allowed to grow to a size of approximately 100 mm^3. Compounds **36** and **41** were selected for in vivo testing because of their significant FLT3 inhibitory activity and MV4-11 antiproliferative activity. A single oral dose of 20 mg/kg of compound **36**, **41** or the PBS control was administered once daily for 21 days. As shown in **Figure 7A**, we found that treatment with both compounds resulted in the rapid and complete remission of tumors in all mice compared with the PBS control group. Particularly, the tumor disappeared by day 14, based on the measured tumor volume. There was no weight loss or any other signs of toxicity during the administration period (**Figure 7B)**. The highly potent in-vivo efficacy of the anti-AML agents, **36** and **41**, by oral administration should be noticeable in terms of generally poor PK profiles of indirubin analogues such as the previously reported compound **9**, of which in-vivo efficacy was similarly achieved with 10 mg/kg dose by intravenous administration only. [25]

Toxicological studies of compound 36

To determine the cardiotoxicity of compound **36**, we performed the hERG potassium channel ligand binding assay along with astemizole as a positive control (**Supporting Table 4**). As the result, compound **36** showed 21.4% inhibition of hERG ligand binding at 10 μM concentration, indicating there is no significant hERG channel related cardiotoxicity. In addition, single-dose toxicity animal experiment was performed to evaluate the lethal dose in acute toxicity when the compound **36** was administered orally to ICR mice (**Supporting Table 5**). During the experiment, one female mouse of the 2,000 mg/kg group died at day 6 and the approximate lethal dose (ALD) is determined over 2,000 mg/kg in male mice and 2,000 mg/kg in female mice, respectively. Median lethal dose (LD_{50}) value was calculated as 4,950 mg/kg in female mice.

Conclusions

In this study, starting from the CDK inhibitor compound **17**, we discovered (2Z,3E)-5'-fluoro-3-((2-(piperazin-1-yl)ethoxy)imino)-[2,3'-biindolinylidene]-2'-one (**36**), a FLT3 inhibitor with a subnanomolar range of IC_{50} values that displayed potent inhibitory activity against the FLT3/D835Y mutation. We optimized the indirubin skeleton through the combination of the best substituents at each position with the aim of increasing the inhibitory activity against FLT3 and the anti-proliferative efficacy of MV4-11 cells. Compound **36** also exhibited significant in vivo antitumor activity in the MV4-11 xenograft animal model and an improved PK profile for oral administration. These results suggest that indirubin-based FLT3 inhibitors could be successful drug candidates for the treatment of AML, which is an important unmet medical need.

Experimental Section

General Methods for Chemistry

The NMR spectra at 400MHz for ^{1}H spectra and 100 MHz for ^{13}C spectra, respectively, were recorded with a JEOL JNM-ECX 400P spectrometer. The other ^{1}H NMR and ^{13}C NMR spectra were obtained on Agilent ProPulse (500 MHz and 125 MHz, respectively) and Varian (600 MHz and 150 MHz, respectively) in Korea Basic Science Institute (KBSI), Gwangju branch. All spectra were taken in $CDCl_3$, DMSO-d_6 or D_2O - solvent. Unless otherwise noted, chemical shifts are expressed as ppm downfield from internal tetramethylsilane (TMS), relative ppm from DMSO reference (2.5 ppm) or HOD reference (4.8 ppm). To identify the solvent-overlapped peak, the NMR spectra of a representative compound, **36**, was recorded using DMSO-d_6 and D_2O (See supporting information). Mass spectroscopy was performed on electrospray method using Waters Quattro micro API (column, Sunfire C18, 100 Å, 3.5 μm, 2.1 × 150 mm; solvent system, 0.1% formic acid in H_2O/0.1% formic acid in CH_3CN = 20:80) by all compounds. High-resolution mass spectra (HRMS) (m/z) of selected compounds were recorded on a fast atom bombardment (FAB) using a JEOL JMS-799 mass spectrometer. High-resolution mass analysis was performed at the Korea Basic Science Institute (Daegu). HPLC analysis were carried out to determine the purity of all final compounds. All compounds showed an HPLC purity of > 95%. The determination of purity was conducted using a Shimadzu SCL-10A VP HPLC system with a Shimadzu Shim-pack C18 analytical column (250 × 4.6 mm, 5 mm, 100 Å) in linear gradient solvent systems (solvent system was H_2O/CH_3CN = 80:20 to 10:90 over 30 min at a flow of 1 mL min−1). Peaks were detected by UV absorption using a diode array detector. The starting materials were purchased from commercial suppliers from Aldrich or TCI. The compounds 12-18 were synthesized according to the previous reports. [23, 24]

tert-butyl (2-((((2Z,3E)-5-hydroxy-5'-nitro-2'-oxo-[2,3'-biindolinylidene]-3-ylidene)amino)oxy)ethyl)carbamate (**19**)

To a solution of indirubin 3′-oxime compound, **17**, (130 mg, 0.38 mmol) and 2-(boc-amino)ethyl bromide (112 mg, 0.5 mmol) in DMF (20 mL) was added K_2CO_3 (138 mg, 1 mmol) and stirred overnight at room temperature. The solvent of reaction mixture was partially evaporated under reduced pressure. The residue was diluted with saturated aq. NH_4Cl (600 mL) and extracted with ethyl acetate (3 × 30 mL). The combined extracts were dried over Na_2SO_4, filtered, and evaporated. The residue was purified by silica gel chromatography (ethyl acetate/n-hexane =1:2) to give **19** (113 mg, 61.8% yield): ^{1}H NMR (CDCl3, 400 MHz) δ 11.65 (s, 1H), 11.38 (s, 1H), 9.57, (s, 1H), 9.35 (s, 1H), 8.07 (d, *J* = 6 Hz, 1H), 7.64 (s, 1H), 7.29 (d, *J* = 5.6 Hz, 1H), 7.05-7.01 (m, 2H), 6.89 (d, *J* = 5.6 Hz, 1H), 4.69 (m, 2H), 3.55 (m, 2H), 1.31 (s, 9H). LC/MS (ESI, m/z) 479.67 $[M - H]^-$.

(2Z,3E)-3-((2-aminoethoxy)imino)-5-hydroxy-5'-nitro-[2,3'-biindolinylidene]-2'-one hydrochloride (**20**)

To s solution of Boc-protected compound **19** (40 mg, 0.08 mmol) in THF (2 mL) at 0 □ was slowly added 4 N HCl in 1,4-dioxane (40 μL, 0.16 mmol) and stirred for 30 min under N_2 atmosphere. The precipitate was collected, washed with DCM, and dried to obtain **20** (32.7 mg, 98% yield). ^{1}H NMR (400MHz, DMSO-d_6) δ 11.66 (s, 1H), 11.47 (s, 1H), 9.51 (d, *J* = 2.4 Hz, 1H), 9.48 (s, 1H), 8.24 (s, 3H), 8.09 (dd, *J* = 8.4, 2.4 Hz, 1H), 7.78 (d, *J* = 2.4 Hz, 1H), 7.30 (d, *J* = 8.4 Hz, 1H), 7.07 (d, *J* = 8.8 Hz, 1H), 6.95 (dd, *J* = 8.4, 2.4 Hz, 1H), 4.87 (t, *J* = 4.4 Hz, 2H), 3.49 (t, *J* = 4.4 Hz, 2H). ^{13}C NMR (100 MHz, DMSO-d_6) δ 171.39, 153.34, 153.37, 146.90, 143.96, 141.74, 138.52, 123.19, 122.37, 120.54, 118.41, 117.10, 116.41, 113.28, 109.12, 97.37, 73.62, 38.40.

(2Z,3E)-3-((2-bromoethoxy)imino)-5'-nitro-[2,3'-biindolinylidene]-2'-one (**21a**)

To a solution of indirubin 3′-oxime compound, **16a**, (100 mg, 0.31 mmol) and TEA (94.1 mg, 0.93 mmol) in DMF (20 mL) was added 1,2-DCE (225 mg, 1.2 mmol) and stirred overnight at room temperature. The crude reaction mixture was evaporated under reduced pressure. The residue was diluted with saturated aq. NH_4Cl (30 mL) and extracted with ethyl acetate (3 × 25 mL). The combined extracts were dried over Na_2SO_4, filtered, and evaporated. The residue was purified by silica gel chromatography (ethyl acetate/n-hexane =1:2) to afford compound **21a**

Yield: 81%. ^{1}H NMR(400MHz, DMSO-d_6) δ 11.75 (s, 1H), 11.48 (s, 1H), 9.64 (d, *J* = 2.4 Hz, 1H), 8.25 (m, 1H), 8.13 (dd, *J* = 8.8, 2.4 Hz, 1H), 7.60 (m, 2H), 7.15-7.09 (m, 2H), 4.99 (m, 2H), 4.05 (m, 2H). LC/MS (ESI, m/z) 429.22 $[M + H]^+$

Compounds **21b-21e** were prepared following the synthetic procedure of compound **21a**.

(2Z,3E)-3-((2-bromoethoxy)imino)-5'-fluoro-[2,3'-biindolinylidene]-2'-one (21b)

Yield: 81%. ^{1}H NMR(400MHz, DMSO-d_6) δ 11.69 (m, 1H), 10.75 (s, 1H), 8.57-8.63 (m, 1H), 8.15 (d, *J* = 7.93 Hz, 1H), 7.40 (d, *J* = 1.24 Hz, 1H), 7.17 (td, *J* = 7.66, 1.22 Hz, 1H), 7.12-7.18 (m, 1H), 6.90-7.01 (m, 1H), 6.85-6.97 (m, 1H), 4.69 (t, *J* = 6.20 Hz, 1H), 2.81-2.96 (m, 2H). LC/MS (ESI, m/z) 402.22 $[M + H]^+$

(2Z,3E)-3-((2-bromoethoxy)imino)-[2,3'-biindolinylidene]-2'-one (21c)

Yield: 80%. ^{1}H NMR(400MHz, DMSO-d_6) δ 11.80 (m, 1H), 10.70 (s, 1H), 8.62 (d, *J* = 7.90 Hz, 1H), 8.15 (d, *J* = 7.61 Hz, 1H), 7.36-7.47 (m, 2H), 7.13 (td, *J* = 7.64, 1.22 Hz, 1H), 7.07 (m, 1H), 6.90-6.96 (m, 1H), 6.89 (d, *J* = 7.67 Hz, 1H), 4.70 (t, *J* = 5.85 Hz, 2H), 2.84 (t, *J* = 6.24 Hz, 2H) . LC/MS (ESI, m/z) 385.23 $[M + H]^+$

(2Z,3E)-3-((2-bromoethoxy)imino)-5'-methoxy-[2,3'-biindolinylidene]-2'-one (21d)

Yield: 77%. ^{1}H NMR(400MHz, DMSO-d_6) δ 11.75 (s, 1H), 10.62 (s, 1H), 8.21 (m, 2H), 7.48-7.40 (m, 2H), 7.07-7.02 (m, 1H), 6.82-6.78 (m, 1H), 6.77-6.73 (m, 1H), 4.88 (t, *J* = 5.48 Hz, 2H), 3.98 (t, *J* = 6.24 Hz, 2H), 3.78 (s, 3H). LC/MS (ESI, m/z) 414.05 $[M + H]^+$

(2Z,3E)-3-((2-bromoethoxy)imino)-5'-(trifluoromethoxy)-[2,3'-biindolinylidene]-2'-one (21e)

Yield: 80%. ^{1}H NMR(400MHz, DMSO-d_6) δ 11.78 (s, 1 H), 10.99 (s, 1 H), 8.59 - 8.55 (m, 1 H), 8.22 (d, *J* = 7.56 Hz, 1 H), 7.49 - 7.45 (m, 2 H), 7.14 (m, *J* = 2.06 Hz, 1 H), 7.08 (m, 1 H), 6.96 (d, *J* = 8.24 Hz, 1 H), 4.86 (t, *J* = 5.72 Hz, 2 H), 3.98 (t, *J* = 5.72 Hz, 2 H). LC/MS (ESI, m/z) 468.01 $[M + H]^+$

(2Z,3E)-3-((2-bromoethoxy)imino)-5-hydroxy-5'-nitro-[2,3'-biindolinylidene]-2'-one (22)

Following the procedure for compound **21a**, **22** (72.7 mg) was obtained from **17** (70 mg, 0.23 mmol). Yield: 60%. ^{1}H NMR (400 MHz, DMSO-d_6) δ 11.60 (s, 1 H), 11.37 (s, 1 H), 9.46 (m, 1 H), 9.42 (s, 1 H), 8.05-8.00 (m, 1 H), 7.61 (m, 1 H), 7.28-7.24 (d, J = 8.48 Hz, 1 H), 7.01-6.97 (d, J = 8.48 Hz, 1 H), 6.89-6.85 (dd, J = 8.72, 2.52 Hz, 1 H), 4.97-4.92 (t, J = 5.52 Hz, 1 H), 4.02-3.97 (t, J = 5.48 Hz, 1 H). ^{13}C NMR (100 MHz, DMSO-d_6) δ 171.41, 153.54, 152.91, 146.83, 143.90, 141.77, 138.65, 123.19, 122.34, 120.75, 118.40, 117.00, 115.63, 113.49, 108.97, 97.47, 76.70, 31.53. LC/MS (ESI, m/z) 445.00 $[M + H]^+$

(2Z,3E)-3-((2-bromoethoxy)imino)-5-fluoro-5'-nitro-[2,3'-biindolinylidene]-2'-one (23a)

Following the procedure for compound **21a**, **23a** (33.8 mg) was obtained from **18a** (125 mg, 0.36 mmol). Yield: 21%. ^{1}H NMR(400MHz, DMSO-d_6) δ 11.75 (s, 1H), 11.29 (s, 1H), 9.53 (s, 1H), 8.11 (dd, *J* = 8.4, 4.0 Hz, 1H), 7.97 (dd, *J* =7.6, 2.0 Hz, 1H), 7.53 (m, 1H), 7.40 (m, 1H), 7.06 (d, *J* = 9.6 Hz, 1H), 5.03 (m, 2H), 4.08 (m, 2H). LC/MS (ESI, m/z) 447.21 $[M + H]^+$.

(2Z,3E)-3-((2-bromoethoxy)imino)-5,5'-difluoro-[2,3'-biindolinylidene]-2'-one (23b)

Following the procedure for compound **21a**, **23b** (72.7 mg) was obtained from **18b** (70 mg, 0.23 mmol). Yield: 67%. ^{1}H NMR(400MHz, DMSO-d_6) δ 11.73 (s, 1H), 10.80 (s, 1H), 8.36 (dd, *J* = 11.2, 2.8 Hz, 1H), 7.99 (dd, *J* = 8.8, 2.8 Hz, 1H), 7.50 (m, 1H), 7.39 (m, 1H), 6.99 (m, 1H), 6.88 (m, 1H), 4.71-4.68 (t, *J* = 5.8 Hz, 2H), 2.87-2.84 (t, *J* = 5.8 Hz, 2H) LC/MS (ESI, m/z) 420.21 $[M+H]^{+}$.

(2Z,3E)-5-hydroxy-5'-nitro-3-((2-(piperazin-1-yl)ethoxy)imino)-[2,3'-biindolinylidene]-2'-one hydrochloride (24)

To a solution of **22** (25 mg, 0.056 mmol) in dried DMF (2.5 mL) was added piperazine (24.2 mg, 0.28 mmol). The reaction mixture was stirred overnight at 50 □. The mixture was cooled to 0 □ before pouring water (2.5 mL) into the reaction flask. The resulting solid was filtered, washed several times with cold water, and dried to provide claret solid. Next, a solution of this material in THF at 0 □, 2 equivalents of 4N HCl in 1,4-dioxane was added, and the reaction mixture was stirred for 30 min. The precipitate was collected, washed with DCM, and dried to obtain **24** (7.75 mg). Yield: 31%. ^{1}H NMR(400MHz, DMSO-d_6) δ 11.65 (s, 1H), 11.46 (s, 1H), 9.54 (d, *J* = 2.4 Hz, 1H), 9.26 (brs, 2H), 8.11-8.08 (dd, *J* = 8.8, 2.4 Hz, 1H), 7.75 (s, 1H), 7.33-7.31 (d, *J* = 8.8 Hz, 1H), 7.08-7.06 (d, *J* = 8.4 Hz, 1H), 6.94-6.92 (dd, *J* = 8.4, 2.4 Hz, 1H), 5.04 (brs, 2H), 3.69 (brs, 10H, partially overlapped with water). ^{1}H NMR(400MHz, D_2O) δ 8.27 (s, 1H), 7.44 (d, *J* = 8 Hz, 1H), 6.69 (s, 1H), 6.53-6.51 (d, *J* = 8 Hz, 1H), 6.40-6.38 (d, *J* = 8 Hz, 1H), 6.32 (d, *J* = 6.4 Hz, 1H), 4.47 (brs, 2H), 3.56-3.42 (m, 10H). ^{13}C NMR (D_2O, 100 MHz) δ 172.04, 146.12, 143.39, 141.90, 140.73, 137.50, 134.92, 125.30, 124.43, 121.87, 121.70, 117.90, 115.50, 114.42, 108.27, 96.50, 71.60, 55.34, 49.30, 41.43. ^{13}C NMR (100 MHz, DMSO-d_6) δ 171.38, 153.78, 146.77, 146.54, 144.00, 141.75, 138.72, 123.16, 122.47, 120.83, 118.38, 116.88, 115.67, 113.63, 109.13, 97.57, 48.87, other

peaks are overlapped in solvent peak or undetected in DMSO-d_6 solvent system. LC/MS (ESI, m/z) 451.17 $[M - Cl]^+$

Compounds **25-49** were prepared following the synthetic procedure of compound **24**

(2Z,3E)-5-hydroxy-3-((2-(4-methylpiperazin-1-yl)ethoxy)imino)-5'-nitro-[2,3'-biindolinylidene]-2'-one hydrochloride (25)

Yield: 81%. ^{1}H NMR (400 MHz, DMSO-d_6) δ 11.65 (s, 1 H), 11.45 (s, 1 H), 9.55-9.48 (m, 2 H), 8.10-8.07 (dd, J = 8.48, 2.32 Hz, 1 H), 7.74 (s, 1 H), 7.32-7.30 (d, J = 8.48 Hz, 1 H), 7.08-7.06 (d, J = 8.48 Hz, 1 H), 6.93-6.91 (dd, J = 8.48, 2.52 Hz, 1 H), 5.00 (m, 2 H), 3.45-3.11 (m, 10 H, overlapped with water peak), 2.79 (s, 3 H). ^{13}C NMR (100 MHz, DMSO-d_6) 171.39, 153.81, 153.78, 146.80, 144.12, 141.77, 138.71, 123.18, 122.45, 120.80, 118.69, 116.90, 115.69, 113.60, 109.10, 97.56, other peaks are overlapped in solvent peak or undetected in DMSO-d_6 solvent system. LC/MS (ESI, m/z) 465.19 $[M - Cl]^+$

(2Z,3E)-5-hydroxy-3-((2-morpholinoethoxy)imino)-5'-nitro-[2,3'-biindolinylidene]-2'-one hydrochloride (26)

Yield: 50%. ^{1}H NMR (400MHz, DMSO-d_6) δ 11.66 (s, 1 H), 11.47 (s, 1 H), 10.90 (brs, 1 H), 9.53 (m, 2 H), 8.11-8.08 (dd, J =8.0, 2.0 Hz, 1 H), 7.72 (d, J = 2 Hz, 1 H), 7.33-7.31 (d, J = 8.8 Hz, 1 H), 7.33.-7.31 (d, J = 8.8 Hz, 1 H), 6.95-6.92 (m, 1 H), 5.11 (m, 2 H), 4.01-3.77 (m, 5 H), 3.55-3.29 (m, 5 H, slightly overlapped in water peak). ^{13}C NMR (100MHz, DMSO-d_6) 171.36, 153.72, 153.30, 146.80, 144.06, 141.80, 138.83, 123.20, 122.54, 120.89, 118.72, 116.94, 115.62, 113.70, 109.16, 97.61, 70.31, 63.89, 54.83, 52.04. LC/MS (ESI, m/z) 452.15 $[M - Cl]^+$

(2Z,3E)-5-fluoro-5'-nitro-3-((2-(piperazin-1-yl)ethoxy)imino)-[2,3'-biindolinylidene]-2'-one hydrochloride (27)

Yield: 43%. ^{1}H NMR(500MHz, D_2O) δ 8.14 (s, 1 H), 7.31 (d, J = 8 Hz, 1 H), 7.06 (d, J = 8 Hz, 1 H), 6.77 (m, 1 H), 6.43 (m, 1 H), 6.14 (d, J = 8.5 Hz, 1 H), 4.41 (brs, 2 H), 3.52 – 3.44 (m, 10 H). ^{13}C NMR (125MHz, D_2O) δ 170.81, 158.89, 156.98, 150.68, 145.41, 142.17, 140.68, 140.08, 122.36, 121.36, 120.18 117.94, 115.06, 112.89, 108.30, 97.55, 71.21, 55.19, 49.14, 41.13 LC/MS (ESI, m/z) 453.17 $[M - Cl]^+$

(2Z,3E)-5-fluoro-3-((2-(4-methylpiperazin-1-yl)ethoxy)imino)-5'-nitro-[2,3'-biindolinylidene]-2'-one hydrochloride (28)

Yield: 52%. ^{1}H NMR(400MHz, DMSO-d_6) δ 9.54 (d, *J* = 2.1 Hz, 1H), 8.09 (m, 1H), 7.95 (dd, *J* = 8.9, 2.4 Hz, 1 H), 7.45 (m, 1 H), 7.31 (m, 1 H), 7.08 (d, J = 8.88 Hz, 1 H), 4.97 (brs, 2H), 3.40 (m, 10H, partially overlapped with water), 2.80 (s, 3H). ^{1}H NMR(400MHz, D_2O) δ 8.28 (s, 1 H), 7.38-7.36 (d, J = 8.4 Hz, 1 H), 7.01-6.99 (d, J = 8.4 Hz, 1 H), 6.79 (m, 1 H), 6.48-6.45 (m, 1 H), 6.26-6.24 (d, J = 7.6 Hz, 1 H), 4.27 (brs, 2H), 3.58-3.05 (m, 10 H), 2.80 (s, 3 H). ^{13}C NMR (100MHz, D_2O) δ 170.35, 160.24, 155.90, 149.84, 145.89, 142.38, 141.69, 140.14, 123.24, 120.05, 118.26, 115.86, 114.52, 112.18, 108.48, 97.46, 72.62, 54.81, 51.96, 49.61, 42.80. LC/MS (ESI, m/z) 468.18 $[M - Cl]^+$

(2Z,3E)-5'-nitro-3-((2-(piperazin-1-yl)ethoxy)imino)-[2,3'-biindolinylidene]-2'-one hydrochloride (29)

Yield: 39%. ^{1}H NMR δ (400 MHz, D_2O) δ 8.22 (s, 1 H), 7.38 (d, J = 7.32 Hz, 1 H), 7.30-7.27 (dd, J = 8.32, 1.48 Hz, 1 H), 7.09-7.05 (t, J = 7.80 Hz, 1 H), 6.77-6.73 (t, J = 7.32 Hz, 1 H), 6.49-6.47 (d, J = 7.80 Hz, 1 H), 6.17 (d, J = 8.32 Hz, 1 H), 4.33 (m, 2 H), 3.47-3.36 (m, 10 H). ^{13}C NMR (100 MHz, D_2O) δ 171.12, 151.31, 145.72, 143.89, 142.27, 140.76, 133.41, 128.11, 122.87, 122.25, 121.70, 118.27, 114.99, 111.24, 108.42, 97.31, 71.46, 55.41, 49.27, 41.35. LC/MS (ESI, m/z) 435.19 $[M - Cl]^+$

(2Z,3E)-5,5'-difluoro-3-((2-(piperazin-1-yl)ethoxy)imino)-[2,3'-biindolinylidene]-2'-one hydrochloride (30)

Yield: 49%. ^{1}H NMR (400MHz, D_2O) δ 7.31 (d, J = 9.6 Hz, 1 H), 7.02 (d, J = 6.4 Hz, 1 H), 6.77 (t, J = 6.8 Hz, 1 H), 6.48 – 6.42 (m, 2 H), 6.22 – 6.19 (m, 1 H), 4.50 (m, 2 H), 3.46 – 3.43 (m, 10 H). ^{13}C NMR (100 MHz, D_2O) δ 171.09, 158.70, 156.97, 144.98, 140.54, 133.19, 122.94, 119.57, 119.07, 116.65, 114.45, 112.35, 111.04, 109.63, 109.35, 101.27, 68.68, 55.46, 49.15, 41.10. LC/MS (ESI, m/z) 426.17 $[M - Cl]^+$

(2Z,3E)-5,5'-difluoro-3-((2-(4-methylpiperazin-1-yl)ethoxy)imino)-[2,3'-biindolinylidene]-2'-one hydrochloride (31)

Yield: 69%. ^{1}H NMR(500 MHz, DMSO-d_6) δ 11.75 (s, 1 H), 10.85 (s, 1 H), 8.33 (d, J = 11 Hz, 1 H), 8.06 (m, 1 H), 7.46 (m, 1 H), 7.36 (m, 1 H), 7.00 (m, 1 H), 6.89 (m, 1 H), 4.97 (m, 2 H), 3.54 – 3.10 (m, 10 H, partially overlapped with water), 2.80 (s, 3 H). ^{13}C NMR (125 MHz, DMSO-d_6) 171.17, 158.79, 156.91, 152.34, 145.05, 142.74, 135.59, 123.68, 120.72, 116.68, 115.14, 113.60, 112.98, 110.67, 109.84, 100.46, other peaks are overlapped in solvent peak or undetected in DMSO-d_6 solvent system. LC/MS (ESI, m/z) 440.19 $[M - Cl]^+$.

(2Z,3E)-5,5'-difluoro-3-((2-(piperidin-4-ylamino)ethoxy)imino)-[2,3'-biindolinylidene]-2'-one hydrochloride (32)

Yield: 54%. ^{1}H NMR(500 MHz, D_2O) δ 7.27-7.25 (d, J = 10.5 Hz, 1 H), 6.98-6.97 (d, J = 7 Hz, 1 H), 6.65-6.62 (t, J = 6.5 Hz, 1 H), 6.44-6.42 (t, *J* = 7.5 Hz, 1 H), 6.3 – 6.32 (dd, J = 8, 3.5 Hz, 1 H), 6.18 – 6.15 (dd, J = 8.5, 5 Hz, 1 H), 4.43 (m, 2 H), 3.62 – 3.29 (m, 5 H), 3.01-2.96 (t, J = 13 Hz, 2 H), 2.32 – 2. 29 (d, J = 13.5 Hz, 1 H), 1.86 – 1.79 (dd, J = 13, 3 Hz, 2 H). ^{13}C NMR (125 MHz, D_2O) δ 170.71, 158.72, 156.88, 156.48, 151.24, 144.84,

140.17, 132.87, 122.25, 119.47, 115.22, 114.65, 112.19, 110.98, 109.46, 99.27, 71.33, 52.73, 43.28, 42.21, 24.97. LC/MS (ESI, m/z) 439.18 $[M - Cl]^+$.

(2Z,3E)-5,5'-difluoro-3-((2-morpholinoethoxy)imino)-[2,3'-biindolinylidene]-2'-one hydrochloride (33)

Yield: 43%. ^{1}H NMR(400MHz, DMSO-d_6) δ 11.70 (s, 1 H), 11.20 (brs, 1 H), 10.81 (s, 1 H), 8.29 – 8.26 (dd, J = 11.6, 2.8 Hz, 1 H), 8.02 – 7.99 (dd, J = 8.4, 2.4 Hz, 1 H), 7.45-7.42 (dd, J = 8.4, 4.4 Hz, 1 H), 7.35-7.32 (td, J = 9.2, 2.8 Hz, 1 H), 6.96-6.93 (td, J = 8.8, 2.8 Hz, 1 H), 6.85-6.82 (dd, J = 8, 4.8 Hz, 1 H), 5.001 (m, 2 H), 3.95-3.92 (m, 2 H), 3.79-3.76 (m, 3 H), 3.51-3.49 (m, 2 H), 3.24-3.22 (m, 3 H, partially overlapped with water). ^{13}C NMR (100MHz, DMSO-d_6) δ 171.22, 159.00, 156.74, 152.48, 145.01, 142.86, 135.67, 123.69, 120.88, 116.65, 115.83, 113.69, 113.05, 110.82, 109.91, 101.13, 71.51, 63.83, 54.76, 51.99. LC/MS (ESI, m/z) 427.18 $[M - Cl]^+$

(2Z,3E)-5,5'-difluoro-3-((2-(piperidin-1-yl)ethoxy)imino)-[2,3'-biindolinylidene]-2'-one hydrochloride (34)

Yield: 20%. ^{1}H NMR(500MHz, DMSO-d_6) δ 11.74 (s, 1 H), 10.84 (s, 1 H), 10.21 (brs, 1 H), 8.33-8.30 (dd, J = 11, 2.5 Hz, 1 H), 8.03-8.00 (dd, J = 8.5, 2.5 Hz, 1 H), 7.49-7.46 (dd, J = 9, 4.5 Hz, 1 H), 7.38-7.35 (td, J = 9, 2.5 Hz, 1 H), 7.01-6.97 (td, J = 8.5, 3 Hz, 1 H), 6.89-6.86 (dd, J = 8.5, 4.5 Hz, 1 H), 5.02-4.99 (t, J = 4.5 Hz, 2 H), 3.70 (m, 2 H), 3.60-3.58 (t, J = 6.5 Hz, 1 H), 3.56-3.52 (m, 2 H), 3.07-3.44 (t, J = 12.5 Hz, 2 H), 1.76-1.65 (m, 5 H). ^{13}C NMR (125MHz, DMSO-d_6) δ 170.68, 158.22, 156.41, 152.00, 144.45, 142.35, 135.16, 123.15, 123.07, 120.36, 116.14, 114.93, 113.22, 112.27, 109.33, 100.60, 71.09, 54.16, 52.53, 22.48, 21.06. LC/MS (ESI, m/z) 425.17 $[M - Cl]^+$

(2Z,3E)-5,5'-difluoro-3-((2-(pyrrolidin-1-yl)ethoxy)imino)-[2,3'-biindolinylidene]-2'-one hydrochloride (35)

Yield: 75%. ^{1}H NMR (600MHz, DMSO-d_6) δ 11.76 (s, 1 H), 10.85 (s, 1 H), 10.25 (brs, 1 H), 8.34-8.32 (dd, J = 11.4, 2.4 Hz, 1 H), 8.06-8.04 (dd, J = 8.4, 2.4 Hz, 1 H), 7.50-7.48 (q, J = 4.2 Hz, 1 H), 7.40-7.36 (td, J = 9, 2.4 Hz, 1 H), 7.03-6.98 (td, J = 9, 3 Hz, 1 H), 6.90-6.87 (q, J = 4.2 Hz, 1 H), 4.95 (t, J = 4.8 Hz, 2 H), 3.82 (q, J = 5.04 Hz, 2 H), 3.69-3.58 (m, 2 H), 3.17-3.11 (m, 2 H), 2.03-1.99 (m, 2 H), 1.90-1.86 (m, 2 H). ^{13}C NMR (150MHz, DMSO-d_6) δ 170.70, 158.09, 156.55, 152.06, 144.49, 142.35, 135.16, 123.16, 120.37, 116.27, 115.20, 113.16, 112.70, 101.17, 109.10, 100.62, 71.72, 53.57, 52.26, 22.56. LC/MS (ESI, m/z) 411.16 $[M - Cl]^+$.

(2Z,3E)-5'-fluoro-3-((2-(piperazin-1-yl)ethoxy)imino)-[2,3'-biindolinylidene]-2'-one hydrochloride (36)

Yield: 77%. ^{1}H NMR (400 MHz, DMSO-d_6) 11.74 (s, 1 H), 10.90 (s, 1 H), 10.17 (m, 2 H), 8.34-8.31 (dd, J = 11.2, 2.96 Hz, 1 H), 8.29 (d, J = 7.80 Hz, 1 H), 7.45-7.43 (m, 2 H), 7.04 (t, J = 7.32 Hz, 1 H), 7.01-6.95 (m, 1 H), 6.91-6.87 (m, 1 H), 5.04 (m, 2 H), 3.85 (m, 2 H, overlapped in solvent peak), 3.78-3.52 (m, 4 H), 3.48 (m, 4 H). ^{13}C NMR (100 MHz, DMSO-d_6) δ 171.26, 153.06, 146.26, 144.97, 135.64, 133.88, 129.58, 123.68, 122.54, 116.38, 113.18, 112.93, 112.55, 110.59, 109.93, 100.85, 71.34, 54.48, 48.70, the other peak is overlapped in solvent peak. ^{13}C NMR (100 MHz, D_2O) 170.99, 158.83, 156.54, 151.77, 144.66, 144.13, 132.99, 128.21, 122.46, 122.04, 115.27, 111.94, 111.67, 110.66, 109.33, 99.31, 69.79, 55.55, 49.17, 40.78. LC/MS (ESI, m/z) 408.18 $[M - Cl]^+$. HRMS (FAB) m/z calculated for $C_{22}H_{23}FN_5O_5$ $[M-Cl]^+$ 408.1836, found 408.1834.

(2Z,3E)-5'-fluoro-3-((2-(4-methylpiperazin-1-yl)ethoxy)imino)-[2,3'-biindolinylidene]-2'-one hydrochloride (37)

Yield: 64%. ^{1}H NMR (400 MHz, D_2O) δ 7.21-7.18 (d, 7.32, 1 H), 7.05-7.02 (dd, 11.6, 2.44, 1 H) 6.95-6.92 (t, J = 7.32, 1 H), 6.59-6.55 (t, J = 7.32 Hz, 1 H), 6.36-6.34 (d, J = 7.84 Hz, 1 H), 6.21-6.16 (m, 1 H), 5.92-5.88 (m, 1 H), 4.20 (m, 2 H), 3.60-3.41 (m, 8 H), 3.35 (m, 2 H), 2.92 (s, 3 H). ^{13}C NMR (100 MHz, D_2O) δ 170.79, 156.43, 151.40, 144.48, 143.98, 132.89, 132.80, 132.73, 128.06, 128.03, 127.87, 121.94, 115.18, 110.59, 109.26, 99.20, 70.25, 55.18, 50.62, 49.49, 42.95. LC/MS (ESI, m/z) 422.19 $[M - Cl]^+$.

(2Z,3E)-5'-fluoro-3-((2-(piperidin-4-ylamino)ethoxy)imino)-[2,3'-biindolinylidene]-2'-one hydrochloride (38)

Yield: 57%. ^{1}H NMR (500MHz, D_2O) δ 7.48-7.46 (d, J = 8 Hz, 1 H), 7.42-7.39 (d, J = 12 Hz, 1 H), 7.05-7.01 (t, J = 7.5 Hz, 1 H), 6.70-6.67 (t, J = 7.5 Hz, 1 H), 6.51-6.48 (d, J = 7.5 Hz, 1 H), 6.47-6.43 (m, 1 H), 6.23-6.20 (dd, J = 8, 5 Hz, 1 H), 4.41 (m, 2 H), 3.51-3.40 (m, 4 H), 2.98-2.89 (t, J = 13 Hz, 1 H), 2.28-2.25 (d, J = 13.5 Hz, 1 H), 1.83-1.74 (m, 3 H). ^{13}C NMR (125 MHz, D_2O) δ 170.12, 157.01, 152.94, 145.17, 144.17, 136.54, 133.04, 130.94, 128.96, 128.54, 126.43, 122.07, 115.43, 110.63, 109.62, 99.25, 71.08, 52.63, 43.36, 42.23, 25.00. LC/MS (ESI, m/z) 421.19 $[M - Cl]^+$.

(2Z,3E)-5'-fluoro-3-((2-(piperidin-1-yl)ethoxy)imino)-[2,3'-biindolinylidene]-2'-one hydrochloride (39)

Yield: 85%. ^{1}H NMR(400MHz, DMSO-d_6) δ 11.76 (s, 1 H), 10.86 (s, 1 H), 10.64 (brs, 1 H), 8.37-8.34 (d, J = 11.2 Hz, 1 H), 8.26-8.21 (d, J = 7.2 Hz, 1 H), 7.46 (m, 2 H), 7.08-6.97 (m, 2 H), 6.90-6.86 (m, 1 H), 5.03 (brs, 2 H), 3.69 (m, 2 H), 3.54-3.52 (d, J = 11.6 Hz, 2 H), 3.06 (m, 2 H), 1.79-1.67 (m, 5 H), 1.38 (m, 1 H). ^{13}C NMR (100 MHz, DMSO-d_6) δ

171.38, 152.92, 146.30, 144.93, 135.62, 133.92, 129.24, 122.44, 116.41, 113.21, 112.69, 112.53, 110.77, 109.92, 109.82, 100.83, 71.46, 54.79, 53.03, 22.99, 21.60. LC/MS (ESI, m/z) 407.19 $[M - Cl]^+$.

(2Z,3E)-5'-fluoro-3-((2-(pyrrolidin-1-yl)ethoxy)imino)-[2,3'-biindolinylidene]-2'-one hydrochloride (40)

Yield: 63%. ^{1}H NMR(400MHz, DMSO-d_6) δ 11.73 (s, 1 H), 10.82 (s, 1 H), 10.59 (brs, 1 H), 8.35-8.32 (d, J = 10.4 Hz, 1 H), 8.22-8.19 (d, J = 7.2 Hz, 1 H), 7.43 (m, 2 H), 7.03-6.94 (m, 2 H), 6.85 (m, 1 H), 4.92 (m, 2 H), 3.77 (m, 2 H), 3.60-3.56 (m, 2 H), 3.09 (m, 2 H), 1.97-1.72 (m, 4 H). ^{13}C NMR (100 MHz, DMSO-d_6) δ 171.39, 156.70, 153.01, 146.30, 144.95, 135.62, 133.94, 129.41, 123.80, 123.69, 122.43, 116.46, 112.70, 110.80, 110.57, 109.91, 100.84, 72.54, 54.32, 52.76, 23.10. LC/MS (ESI, m/z) 393.17 $[M - Cl]^+$.

(2Z,3E)-3-((2-(piperazin-1-yl)ethoxy)imino)-[2,3'-biindolinylidene]-2'-one hydrochloride (41)

Yield: 72%. ^{1}H NMR(400MHz, DMSO-d_6) δ 11.65 (s, 1H), 10.78 (s, 1H), 8.56 (d, *J* = 7.8 Hz, 1H), 8.17 (m, 1 H), 7.42 (m, 2 H), 7.13 (t, *J* = 7.6, 1 H), 6.99 (m, 2 H), 6.88 (d, J = 7.84 Hz, 1 H), 4.8 (m, 2 H), 3.20-2.60 (m, 10 H, overlapped in water peak). ^{13}C NMR (100 MHz, DMSO-d_6) δ 170.83, 152.00, 145.66, 143.69, 138.79, 133.03, 128.56, 126.52, 123.35, 122.25, 121.49, 120.71, 116.09, 11.83, 109.05, 100.43, 49.05, 42.72 ethyl linker peaks are undetected in DMSO-d6 solvent system. LC/MS (ESI, m/z) 390.19 $[M - Cl]^+$. HRMS (FAB) m/z calculated for $C_{22}H_{24}N_5O_5$ $[M-Cl]^+$ 390.1930, found 390.1932.

(2Z,3E)-3-((2-(4-methylpiperazin-1-yl)ethoxy)imino)-[2,3'-biindolinylidene]-2'-one hydrochloride (42)

Yield: 56%. ^{1}H NMR (400 MHz, D_2O) δ 7.73 (d, J = 7.80 Hz, 1 H), 7.44 (d, J = 7.80 Hz, 1 H), 7.04 (t, J = 8.24 Hz, 6.85 (t, J = 7.32 Hz, 1 H), 6.71-6.64 (m, 2 H), 6.52-6.46 (m, 2 H), 4.33 (m, 2 H), 3.48-3.37 (m, 10 H), 2.84 (s, 3 H). ^{13}C NMR (100 MHz, D_2O) δ 171.27, 144.58, 144.50, 137.11, 132.86, 128.31, 126.20, 123.19, 121.94, 121.85, 121.78, 121.19, 115.34, 110.65, 109.37, 99.69, 70.04, 55.29, 50.51, 49.33, 42.82. LC/MS (ESI, m/z) 404.21 $[M - Cl]^+$.

(2Z,3E)-3-((2-(piperidin-4-ylamino)ethoxy)imino)-[2,3'-biindolinylidene]-2'-one hydrochloride (43)

Yield: 81%. ^{1}H NMR (400 MHz, DMSO-d_6) δ 11.64 (s, 1 H), 10.81 (s, 1 H), 8.50 (d, J = 4.12 Hz, 1 H), 8.45 (m, 2 H), 8.18 (d, J = 7.76 Hz, 1 H), 7.42-7.34 (m, 2 H), 7.14-7.11 (t, J = 7.80 Hz, 1 H), 7.01-6.97 (m, 1 H), 5.14 (m, 2 H), 3.70-3.12 (m, 7 H, partially overlapped with water), 2.12-1.99 (m, 4 H). ^{13}C NMR (100 MHz, DMSO-d_6) δ 171.34, 152.87, 146.36, 144.01, 139.39, 133.76, 129.31, 127.15, 124.15, 122.67, 122.16, 121.43, 116.49, 112.38, 109.61, 101.30, 71.22, 54.83, 50.82, 45.48, 27.55. LC/MS (ESI, m/z) 403.20 $[M - Cl]^+$.

(2Z,3E)-3-((2-(piperidin-1-yl)ethoxy)imino)-[2,3'-biindolinylidene]-2'-one hydrochloride (44)

Yield: 86%. ^{1}H NMR (400 MHz, DMSO-d_6) δ 11.65 (s, 1 H), 10.79-10.76 (m, 2 H), 8.53 (d, J = 7.80 Hz, 1 H), 8.17 (d, J = 7.80 Hz, 1 H), 7.44-7.37 (m, 2 H), 7.15-7.11 (td, J = 8.24, 0.92 Hz, 1 H), 7.02-6.97 (m, 2 H), 6.88 (d, J = 7.76 Hz, 1 H), 5.01 (t, J = 5.04, 2 H), 3.63-3.59 (q, J = 5.04 Hz, 2 H),. 3.52-3.45 (m, 2 H), 3.05-2.98 (m, 2 H), 1.79-1.61 (m, 5 H), 1.39-1.28 (m, 1 H). ^{13}C NMR (100 MHz, DMSO-d_6) δ 171.35, 152.83, 146.39, 144.01, 139.40, 133.77, 129.21, 127.17, 124.05, 123.53, 122.69, 122.04, 121.39, 112.44, 109.57, 101.31, 71.34, 54.91, 53.03, 22.95, 21.61. LC/MS (ESI, m/z) 389.19 $[M - Cl]^+$.

(2Z,3E)-3-((2-(pyrrolidin-1-yl)ethoxy)imino)-[2,3'-biindolinylidene]-2'-one hydrochloride (45)

Yield: 67%. ^{1}H NMR(400MHz, DMSO-d_6) δ 11.66 (s, 1 H), 10.79 (brs, 2 H), 8.52 (d, J = 7.6 Hz, 1 H), 8.20 (d, J = 7.6 Hz, 7.45-7.38 (m, 2 H), 7.16-7.11 (t, J = 8 Hz, 1 H), 7.03-6.97 (m, 2 H), 6.89-6.87 (d, J = 8 Hz, 1 H), 4.94 (m, 2 H), 3.73-3.71 (m, 2 H), 3.60-3.53 (m, 2 H), 3.09-3.05 (t, J = 8 Hz, 2 H), 2.05-1.70 (m, 4 H). ^{13}C NMR (100 MHz, DMSO-d_6) δ 171.35, 152.90, 146.39, 144.02, 139.39, 133.78, 129.38, 127.17, 124.05, 122.70, 122.03, 121.39, 116.54, 112.43, 109.58, 101.30, 72.36, 54.22, 52.86, 23.12. LC/MS (ESI, m/z) 375.18 $[M - Cl]^+$.

(2Z,3E)-5'-methoxy-3-((2-(piperazin-1-yl)ethoxy)imino)-[2,3'-biindolinylidene]-2'-one hydrochloride (46)

Yield: 48%. ^{1}H NMR (400 MHz, DMSO-d_6) δ 11.73 (s, 1 H), 10.61 (s, 1 H), 8.25 (d, J = 7.32 Hz, 1 H), 8.20 (m, 1 H), 7.43-7.37 (m, 2 H), 6.98 (t, J = 6.36 Hz, 1 H), 6.78 (d, J = 8.80 Hz, 1 H), 6.73 (dd, J = 8.28, 2.44 Hz, 1 H), 4.80 (m, 2 H), 3.60-3.37 (m, 10 H), 2.77 (s, 3 H). ^{13}C NMR (100 MHz, D_2O) δ 170.84, 152.96, 151.58, 143.97, 132.79, 128.11, 122.32, 121.61, 120.96, 113.56, 112.01, 110.49, 109.07, 108.95, 107.52, 100.15, 69.97, 55.59, 54.90, 48.87, 40.81. LC/MS (ESI, m/z) 420.21 $[M - Cl]^+$.

(2Z,3E)-5'-methoxy-3-((2-(4-methylpiperazin-1-yl)ethoxy)imino)-[2,3'-biindolinylidene]-2'-one hydrochloride (47)

Yield: 43%. ^{1}H NMR (400 MHz, DMSO-d_6) 11.72 (s, 1 H), 10.61 (s, 1 H), 9.69 (m, 2 H), 8.24 (d, J = 7.32 Hz, 1 H), 8.19 (d, 2.92 Hz, 1 H), 7.44-7.36 (m, 2 H), 6.99 (t, J = 7.32 Hz, 1 H), 6.79-6.77 (d, J = 8.76 Hz, 1 H), 6.74-6.71 (dd, J = 8.80, 2.92 Hz, 1 H), 4.98 (m, 2 H), 3.76-3.55 (m, 13 H, partially overlapped with water). ^{13}C NMR (100 MHz, DMSO-d_6) δ

171.48, 154.87, 153.09, 146.32, 144.04, 133.79, 133.23, 129.59, 123.32, 122.11, 116.51, 113.74, 112.39, 109.94, 109.28, 102.00, 71.69, 56.09, 54.64, 48.88, the other peak is overlapped with solvent peak. LC/MS (ESI, m/z) 434.21 $[M - Cl]^+$.

(2Z,3E)-3-((2-(piperazin-1-yl)ethoxy)imino)-5'-(trifluoromethoxy)-[2,3'-biindolinylidene]-2'-one hydrochloride (48)

Yield: 55%. ^{1}H NMR(400MHz, D_2O) δ 7.53 (m, 2H), 7.03-7.00 (t, J = 7.2 Hz, 1H), 6.76-6.72 (t, J = 7.2 Hz, 1H), 6.60-6.58 (d, J = 8.4 Hz , 1H), 6.38-6.36 (d, J = 7.6 Hz , 1H), 6.26-6.24 (d, J = 8.4, 1H), 4.34 (brs, 2H), 3.74-3.55 (m, 10H). ^{13}C NMR (100MHz, D_2O) δ 171.43, 151.95, 148.02, 145.23, 145.15, 142.00, 135.32, 133.07, 128.16, 122.36, 122.02, 118.76, 115.70, 115.31, 112.15, 109.50, 98.81, 70.33, 55.48, 49.03, 41.06. LC/MS (ESI, m/z) 474.18 $[M - Cl]^+$.

(2Z,3E)-3-((2-(4-methylpiperazin-1-yl)ethoxy)imino)-5'-(trifluoromethoxy)-[2,3'-biindolinylidene]-2'-one hydrochloride (49)

Yield: 62%. ^{1}H NMR(400MHz, DMSO-d_6) δ 11.75 (s, 1 H), 10.99 (s, 1 H), 9.62 (m, 2 H), 8.50 (s, 1 H), 8.24 (d, J = 7.80, 1 H), 7.44-7.41 (m, 2 H), 7.13-7.10 (m, 1 H), 7.43-7.00 (m, 1 H), 6.94 (d, J = 8.28 Hz, 1 H), 4.92 (m, 2 H), 3.59-3.37 (m, 13 H, overlapped in solvent peak). ^{13}C NMR (100 MHz, DMSO-d_6) δ 171.35, 153.09, 146.23, 145.32, 142.98, 138.08, 133.92, 129.55, 123.67, 122.64, 119.88, 119.71, 116.55, 116.46, 112.72, 110.01, 100.20, 54.72, 48.89, other peaks are overlapped in solvent peak or undetected in DMSO-d_6 solvent system. LC/MS (ESI, m/z) 488.20 $[M - Cl]^+$.

In vitro FLT3 kinase assay

The inhibition of the FLT3 kinase activity was measured with homogeneous, time-resolved fluorescence (HTRF) assays. Recombinant proteins containing the FLT3 kinase

domain were purchased from Carna biosciences (Japan). Optimal enzyme, ATP, and substrate concentrations were established with the HTRF KinEASE kit (Cisbio, France) according to the manufacturer's instructions. The FLT3 enzymes were mixed with serially diluted compounds and peptide substrates in a kinase reaction buffer (50 mM HEPES (pH 7.0), 500 μM ATP, 0.1 mM sodium orthovanadate, 5 mM $MgCl_2$, 1 mM DTT, 0.01% bovine serum albumin (BSA), and 0.02% NaN_3). After the addition of the reagents for detection, the TR-FRET signal was measured with a Victor multilabel reader (Perkin Elmer, Waltham, MA, USA). The IC_{50} value was calculated with nonlinear regression using Prism version 5.01 (GraphPad). Ten microliters of the total volume of the kinase reaction were added to the wells of a 96-well assay plate. The kinase reactions were incubated for 90 min. at 25°C and stopped by the addition of 10 mM EDTA. For the detection of the phospho-substrate, the Eu-anti-phosphop70S6K (Thr389) antibody diluted in detection buffer was added to a final concentration of 2 nM, and the reactions were then incubated for 1 h at 25°C. The signal was measured on an EnVision multi-label reader.

Cell Culture

MV4-11 human acute myeloid leukemia cells were purchased from the American Type culture collection (ATCC). The cells were maintained in DMEM medium (Sigma Co., St. Louis, MO, USA) with 10% Fetal bovine serum and 1% pencillin/streptomycin in a humidified incubator at 37°C with 5% CO_2. K562 chronic myeloid leukemia cells were purchased from the ATCC. The cells were maintained in DMEM medium (Hyclone) with 10% Fetal bovine serum (Gibco). MOLM14(ITD, ITD-D835Y, ITD-F691L) were purchased from the ATCC and the cells were maintained in RPMI medium (Hyclone) with 10% Fetal bovine serum (Gibco).

Cytotoxicity assay protocol of MV4-11 cells

10,000 Cells were plated in 96-well plates in 100 μL fresh medium (DMEM containing 10% FBS) and serial dilutions of compounds were added. Test 96-well plates were incubated at 37°C with 5% CO_2 for 72 h. After 72 h incubation, 10 μL of the EZ-Cytox kit reagent from EZ-cytox Cell viability assay kit (DaeilLab, Korea) were added to each well of the 96-well plate and then incubated at 37°C with 5% CO_2 for 3 h. After 3h incubation, metabolically active cells were measured spectrophotometrically at a wavelength of 450 nm with a Victor multilabel reader (Perkin Elmer, Waltham, MA, USA). The IC50 values were calculated with nonlinear regression analysis using OriginPro 9.1 software (OriginLab, Northampton, MA).

Site-directed mutagenesis and viral infection.

Mutagenesis is performed in FLT3-ITD plasmid using Q5 site-directed mutagenesis kit (E0554S). D835Y, F691L mutations were introduced into FLT3-ITD plasmid according to the manufacturer's protocol. HEK293T cells were transfected with plasmid DNA using Polyplus Reagent (114-07) according to manufacturer's instructions. Experiments were performed 24-48 hr after transfection. Lentiviral particles were produced by transiently transfecting HEK293T cells with lentiviral vectors together with packaging vectors, pMD2.G and psPAX2. 48h after transfection, media containing viral particles were collected and filtered for infection. Viral particles were infected to MOLM14 cells and 48 h after infection, infected cells were selected with puromycin (1μg/mL).

Cell proliferation assay

Cell proliferation was assessed by MTT assay against various MOLM14 cells according to the manufacturer´s recommendations (11465007001, Roche)

Molecular Docking

The X-ray crystal structure of FLT3 was obtained from Protein data bank (PDB code: 1RJB) as the template. In order to replace the DFG-out motif with a DFG-in motif from structural template, cFMS X-ray structure (PDB code: 3LCD) was chosen as a second template structure. On the basis of above-mentioned two templates, the DFG-in model of FLT3 was constructed by Discovery Studio 3.5/MODELER algorithm with a maxim level of loop optimization. After construction, the protein was prepared using Prepare protein protocol and a radius of 13 Å around the ATP binding pocket was set as a binding site.

In vivo pharmacokinetic study

Five-week-old adult male ICR mice were used in the present study. Animals were housed four per cage and kept in a vivarium maintained the temperature at 23 ± 2°C and the humidity at 50 ± 10% with a 12 h: 12 h alternating light/dark cycle. All mice were provided food and water ad libitum and were maintain for a week of adaption. On the morning of the test, the mice were anesthetized with Zoletil 50 diluent of Rompun, and the selected compounds were administered via the jugular vein and orally at a dose of 10 mg/kg. Animal blood samples were collected using (RaturnTM, BASi, West Lafayette, IN, USA) and the time point were as follows: for intravenous administration groups (iv), 1, 5, 15, 30, 60, 90, 120, 180, 240, 360, 480, 600, 720, 840 and 1440 min after administration; for oral administration (po), 5, 15, 30, 60, 90, 120, 180, 240, 360, 480, 600, 720, 840 and 1440 min after administration. The collected blood samples were centrifuged at 12,000 rpm and separated plasma was stored at -80°C before analysis. Sample analysis was conducted by validated LC-MS/MS method. The liquid chromatographic system was Ultimate® 3000 HPLC unit (Dionex, Sunnyvale, CA, USA) which connected to AB SCIEX API 3200 triple quadrupole mass spectrometer (Applied Biosystems Sciex, Toronto, Ontario, Canada) with

an electrospray ionization (ESI). All experimental procedures were approved by Dankook University's Institutional Animal Care and Use Committee (DUIACUC).

Western blot analysis

MV4-11 Cells were lysed in SDS Lysis buffer (12 mM Tris-Cl, pH 6.8, 5% glycerol, and 0.4% SDS), and the protein concentrations were measured with the SMART BCA Protein Assay kit (iNtRON Biotechnology, Korea). The proteins were resolved with SDS-polyacrylamide gel electrophoresis followed by transfer to PVDF membranes (Millipore, Billerica, MA, USA) and incubated overnight with the appropriate antibodies. The antibodies used were as follows: STAT5 (#sc-835; 1:1,000) from Santa Cruz (Santa Cruz, CA, USA), phospho-STAT5 (p-STAT5; #9351; 1:1,000) from cell signaling (Cell Signaling Technology, MA, USA), Erk1/2 (#sc-135900; 1:1,000) from Santa Cruz, phospho-Erk1/2 (p-Erk1/2; #4370; 1:1,000) from Cell Signaling Technology and β-actin (#A5441, 1:5,000) from Sigma-Aldrich. Goat anti-rabbit IgG (#111-035-003; 1:5,000) and anti-mouse IgG (#115-035-033; 1:5,000) secondary antibodies were obtained from Jackson ImmunoResearch Laboratories, Inc. (West Grove, PA, USA).

Mouse tumor xenograft

MV-4-11 cells were inoculated subcutaneously in the flank of female BALB/c nu/nu (athymic nude) mice (5 × 106 cells per mouse). When the tumor reached a mean volume of 100 mm^3 (approximately 14 days after inoculation), the mice were randomly divided into three groups (n = 10 for the control group and n = 6 for the compound **36** and **41** test groups) and 10 ml/kg of compound **36**, **41** in PBS, or pure PBS (control) were orally administrated. The drug or the control PBS was administered daily for a duration of 21 days. Tumor sizes were measured twice a week for 21 days, and the tumor volumes were calculated with the following formula: V (volume) = X (length) × D $(width)^2/2$. After 21 days, the mice were

sacrificed, and the tumor weights were measured. All experiments were approved by the Institutional Animal Care and Use Committee of Korea Institute of Toxicology (KIT) and conducted according to the guidelines of Association for Assessment and Accreditation of Laboratory Animal Care International.

FLT3-ITD binding affinity assay

FLT-ITD binding affinity assay was processed by LanthaScreen EU kinase binding assay service (Thermofisher scientific)

AUTHOR INFORMATION

Corresponding Author

*(S.-Y.H.) Phone: +82-52-762-7369. Fax: +82-62-772-2429. Email: syhan@gnu.ac.kr

*(Y.-C.K.) Phone: +82-62-715-2502. Fax: +82-62-715-2484. Email: yongchul@gist.ac.kr.

ACKNOWLEDGMENTS

This research was supported by the Bio & Medical Technology Development Program of the NRF funded by the Korean government, MSIP (NRF-2015M3A9C6030838), and Basic Science Research Program (2018R1A2B6002081) through the National Research Foundation (NRF) funded by the Ministry of Science and IC.

ABBREVIATIONS USED

ATP, adenosin-5′-triphosphate; Boc, *tert*-butylcarnobyl; CDK, cyclin-dependent kinase; 1,2-DCE, 1,2-dichloroethane; DCM, dichloromethane; DMEM, Dulbecco's Modified Eagle Medium; DMF, dimethylformamide; DMSO, dimethyl sulfoxide; EDTA,

ethylenediaminetetraacetic acid; HCl, hydrogen chloride; HEPES, 4-(2-hydroxyethyl)-1-piperazineethanesulfonic acid; HPLC, high-pressure liquid chromatography; HRMS, high-resolution mass spectrometry; NMR, nuclear magnetic resonance; SAR, structure-activity relationship; TEA, triethylamine; TFA, trifluoroacetic acid; THF, tetrahydrofuran; TR-FRET, time-resolved fluorescence energy transfer;

References

[1] S. Takahashi, Downstream molecular pathways of FLT3 in the pathogenesis of acute myeloid leukemia: biology and therapeutic implications, Journal of hematology & oncology, 4 (2011) 13.
[2] S. Zhang, S. Fukuda, Y. Lee, G. Hangoc, S. Cooper, R. Spolski, W.J. Leonard, H.E. Broxmeyer, Essential role of signal transducer and activator of transcription (Stat) 5a but not Stat5b for Flt3-dependent signaling, Journal of Experimental Medicine, 192 (2000) 719-728.
[3] S.E. Mullican, S. Zhang, M. Konopleva, V. Ruvolo, M. Andreeff, J. Milbrandt, O.M. Conneely, Abrogation of nuclear receptors Nr4a3 andNr4a1 leads to development of acute myeloid leukemia, Nature medicine, 13 (2007) 730.
[4] K.M. Sakamoto, S. Grant, D. Saleiro, J.D. Crispino, N. Hijiya, F. Giles, L. Platanias, E.A. Eklund, Targeting novel signaling pathways for resistant acute myeloid leukemia, Molecular genetics and metabolism, 114 (2015) 397-402.
[5] K. Faulk, L. Gore, T. Cooper, Overview of therapy and strategies for optimizing outcomes in de novo pediatric acute myeloid leukemia, Pediatric Drugs, 16 (2014) 213-227.
[6] C.G.A.R. Network, Genomic and epigenomic landscapes of adult de novo acute myeloid leukemia, New England Journal of Medicine, 368 (2013) 2059-2074.
[7] E. Papaemmanuil, M. Gerstung, L. Bullinger, V.I. Gaidzik, P. Paschka, N.D. Roberts, N.E. Potter, M. Heuser, F. Thol, N. Bolli, Genomic classification and prognosis in acute myeloid leukemia, New England Journal of Medicine, 374 (2016) 2209-2221.
[8] M. Nakao, S. Yokota, T. Iwai, H. Kaneko, S. Horiike, K. Kashima, Y. Sonoda, T. Fujimoto, S. Misawa, Internal tandem duplication of the flt3 gene found in acute myeloid leukemia, Leukemia, 10 (1996) 1911-1918.
[9] Y. Yamamoto, H. Kiyoi, Y. Nakano, R. Suzuki, Y. Kodera, S. Miyawaki, N. Asou, K. Kuriyama, F. Yagasaki, C. Shimazaki, Activating mutation of D835 within the activation loop of FLT3 in human hematologic malignancies, Blood, 97 (2001) 2434-2439.
[10] N. Mulet-Margalef, X. Garcia-del-Muro, Sunitinib in the treatment of gastrointestinal stromal tumor: patient selection and perspectives, OncoTargets and therapy, 9 (2016) 7573.
[11] T. Fischer, R.M. Stone, D.J. DeAngelo, I. Galinsky, E. Estey, C. Lanza, E. Fox, G. Ehninger, E.J. Feldman, G.J. Schiller, Phase IIB trial of oral Midostaurin (PKC412), the FMS-like tyrosine kinase 3 receptor (FLT3) and multi-targeted kinase inhibitor, in patients with acute myeloid leukemia and high-risk myelodysplastic syndrome with either wild-type or mutated FLT3, Journal of Clinical Oncology, 28 (2010) 4339.
[12] H. Kiyoi, Flt3 inhibitors: recent advances and problems for clinical application, Nagoya journal of medical science, 77 (2015) 7.

[13] L.M. Kelly, J.-C. Yu, C.L. Boulton, M. Apatira, J. Li, C.M. Sullivan, I. Williams, S.M. Amaral, D.P. Curley, N. Duclos, CT53518, a novel selective FLT3 antagonist for the treatment of acute myelogenous leukemia (AML), Cancer cell, 1 (2002) 421-432.
[14] P.P. Zarrinkar, R.N. Gunawardane, M.D. Cramer, M.F. Gardner, D. Brigham, B. Belli, M.W. Karaman, K.W. Pratz, G. Pallares, Q. Chao, AC220 is a uniquely potent and selective inhibitor of FLT3 for the treatment of acute myeloid leukemia (AML), Blood, 114 (2009) 2984-2992.
[15] J.M. Gozgit, M.J. Wong, S. Wardwell, J.W. Tyner, M.M. Loriaux, Q.K. Mohemmad, N.I. Narasimhan, W.C. Shakespeare, F. Wang, B.J. Druker, Potent activity of ponatinib (AP24534) in models of FLT3-driven acute myeloid leukemia and other hematologic malignancies, Molecular cancer therapeutics, 10 (2011) 1028-1035.
[16] C.C. Smith, E.A. Lasater, K.C. Lin, Q. Wang, M.Q. McCreery, W.K. Stewart, L.E. Damon, A.E. Perl, G.R. Jeschke, M. Sugita, Crenolanib is a selective type I pan-FLT3 inhibitor, Proceedings of the National Academy of Sciences, 111 (2014) 5319-5324.
[17] L.Y. Lee, D. Hernandez, T. Rajkhowa, S.C. Smith, J.R. Raman, B. Nguyen, D. Small, M. Levis, Preclinical studies of gilteritinib, a next-generation FLT3 inhibitor, Blood, 129 (2017) 257-260.
[18] B.D. Smith, M. Levis, M. Beran, F. Giles, H. Kantarjian, K. Berg, K.M. Murphy, T. Dauses, J. Allebach, D. Small, Single-agent CEP-701, a novel FLT3 inhibitor, shows biologic and clinical activity in patients with relapsed or refractory acute myeloid leukemia, Blood, 103 (2004) 3669-3676.
[19] M. Levis, P. Brown, B.D. Smith, A. Stine, R. Pham, R. Stone, D. DeAngelo, I. Galinsky, F. Giles, E. Estey, Plasma inhibitory activity (PIA): a pharmacodynamic assay reveals insights into the basis for cytotoxic response to FLT3 inhibitors, Blood, 108 (2006) 3477-3483.
[20] C.C. Smith, Q. Wang, C.-S. Chin, S. Salerno, L.E. Damon, M.J. Levis, A.E. Perl, K.J. Travers, S. Wang, J.P. Hunt, Validation of ITD mutations in FLT3 as a therapeutic target in human acute myeloid leukaemia, Nature, 485 (2012) 260.
[21] P. Polychronopoulos, P. Magiatis, A.-L. Skaltsounis, V. Myrianthopoulos, E. Mikros, A. Tarricone, A. Musacchio, S.M. Roe, L. Pearl, M. Leost, Structural basis for the synthesis of indirubins as potent and selective inhibitors of glycogen synthase kinase-3 and cyclin-dependent kinases, Journal of medicinal chemistry, 47 (2004) 935-946.
[22] D. Marko, S. Schätzle, A. Friedel, A. Genzlinger, H. Zankl, L. Meijer, G. Eisenbrand, Inhibition of cyclin-dependent kinase 1 (CDK1) by indirubin derivatives in human tumour cells, British journal of cancer, 84 (2001) 283.
[23] S.J. Choi, M.J. Moon, S.D. Lee, S.-U. Choi, S.-Y. Han, Y.-C. Kim, Indirubin derivatives as potent FLT3 inhibitors with anti-proliferative activity of acute myeloid leukemic cells, Bioorganic & medicinal chemistry letters, 20 (2010) 2033-2037.
[24] S.-J. Choi, J.-E. Lee, S.-Y. Jeong, I. Im, S.-D. Lee, E.-J. Lee, S.K. Lee, S.-M. Kwon, S.-G. Ahn, J.-H. Yoon, 5, 5′-substituted indirubin-3′-oxime derivatives as potent cyclin-dependent kinase inhibitors with anticancer activity, Journal of medicinal chemistry, 53 (2010) 3696-3706.
[25] H.J. Lee, J. Lee, P. Jeong, J. Choi, J. Baek, S.J. Ahn, Y. Moon, J.D. Heo, Y.H. Choi, Y.-W. Chin, Discovery of a FLT3 inhibitor LDD1937 as an anti-leukemic agent for acute myeloid leukemia, Oncotarget, 9 (2018) 924.
[26] S. Eid, S. Turk, A. Volkamer, F. Rippmann, S. Fulle, KinMap: a web-based tool for interactive navigation through human kinome data, BMC bioinformatics, 18 (2017) 16.
[27] J. Gotlib, D.J. DeAngelo, T.I. George, C.L. Corless, A. Linder, C. Langford, C. Dutreix, S. Gross, Z. Nikolova, T. Graubert, KIT inhibitor midostaurin exhibits a high rate of

clinically meaningful and durable responses in advanced systemic mastocytosis: report of a fully accrued phase II trial, in, Am Soc Hematology, 2010.
[28] A. Galanis, M. Levis, Inhibition of c-Kit by tyrosine kinase inhibitors, Haematologica, 100 (2015) e77.
[29] F.G. Perabo, C. Froessler, G. Landwehrs, D.H. Schmidt, A. Von Ruecker, A. Wirger, S.C. Mueller, Indirubin-3′-monoxime, a CDK inhibitor induces growth inhibition and apoptosis-independent up-regulation of survivin in transitional cell cancer, Anticancer research, 26 (2006) 2129-2135.
[30] J.-W. Lee, M.J. Moon, H.-Y. Min, H.-J. Chung, E.-J. Park, H.J. Park, J.-Y. Hong, Y.-C. Kim, S.K. Lee, Induction of apoptosis by a novel indirubin-5-nitro-3′-monoxime, a CDK inhibitor, in human lung cancer cells, Bioorganic & medicinal chemistry letters, 15 (2005) 3948-3952.
[31] M.J. Moon, S.K. Lee, J.-W. Lee, W.K. Song, S.W. Kim, J.I. Kim, C. Cho, S.J. Choi, Y.-C. Kim, Synthesis and structure–activity relationships of novel indirubin derivatives as potent anti-proliferative agents with CDK2 inhibitory activities, Bioorganic & medicinal chemistry, 14 (2006) 237-246.
[32] D. Staudt, H. Murray, T. McLachlan, F. Alvaro, A. Enjeti, N. Verrills, M. Dun, Targeting oncogenic signaling in mutant FLT3 acute myeloid leukemia: the path to least resistance, International journal of molecular sciences, 19 (2018) 3198.
[33] M. Larrosa-Garcia, M.R. Baer, FLT3 inhibitors in acute myeloid leukemia: current status and future directions, Molecular cancer therapeutics, 16 (2017) 991-1001.
[34] M. Mori, N. Kaneko, Y. Ueno, M. Yamada, R. Tanaka, R. Saito, I. Shimada, K. Mori, S. Kuromitsu, Gilteritinib, a FLT3/AXL inhibitor, shows antileukemic activity in mouse models of FLT3 mutated acute myeloid leukemia, Investigational new drugs, 35 (2017) 556-565.
[35] Y.-Y. Ke, V.K. Singh, M.S. Coumar, Y.C. Hsu, W.-C. Wang, J.-S. Song, C.-H. Chen, W.-H. Lin, S.-H. Wu, J.T. Hsu, Homology modeling of DFG-in FMS-like tyrosine kinase 3 (FLT3) and structure-based virtual screening for inhibitor identification, Scientific reports, 5 (2015) 11702.
[36] S.R. Hubbard, J.H. Till, Protein tyrosine kinase structure and function, Annual review of biochemistry, 69 (2000) 373-398.
[37] A.P. Kornev, N.M. Haste, S.S. Taylor, L.F. Ten Eyck, Surface comparison of active and inactive protein kinases identifies a conserved activation mechanism, Proceedings of the national academy of sciences, 103 (2006) 17783-17788.
[38] J.A. Zorn, Q. Wang, E. Fujimura, T. Barros, J. Kuriyan, Crystal structure of the FLT3 kinase domain bound to the inhibitor quizartinib (AC220), PloS one, 10 (2015) e0121177.

Highlights

1. We discovered an orally active, potent and novel FLT3 and FLT3/D835Y inhibitor, compound **36**, with IC_{50} value of 0.87 and 0.32 nM, respectively, through the optimization of the kinase inhibitory activities and PK profiles.

2. In the molecular docking studies, the inhibitors were interacted and bound into the ATP binding pocket as Type 1 kinase inhibitors and the detailed analysis of the mode of binding was discussed.

3. The kinase selectivity profile was analyzed with an oncology kinase panel.

4. The novel inhibitor also showed potent anti-AML efficacy at FLT3-ITD expressed MV4;11 AML cells, FLT3/D835Y and FLT3/F69L expressed MOLM14 cells with IC_{50} values of 1.0, 1.87 and 3.27 nM, respectively.

5. In the xenograft animal models with MV4;11 cell transplantation, the inhibitor completely suppressed the tumor progression by oral administration of 20 mg/kg once daily dosing schedule for 21 days.

Declaration of interests

☒ The authors declare that they have no known competing financial interests or personal relationships that could have appeared to influence the work reported in this paper.

☐The authors declare the following financial interests/personal relationships which may be considered as potential competing interests: